

GPO PRICE \$ _____

CFSTI PRICE(S) \$ _____

Hard copy (HC) 2.00

Microfiche (MF) .50

ff 653 July 65

N67 13131

FACILITY FORM 602

(ACCESSION NUMBER)

43

(PAGES)

CR-80482

(NASA CR OR TMX OR AD NUMBER)

(THRU)

1

(CODE)

33

(CATEGORY)

**Therm
Advanced
Research, Inc.**

100 HUDSON CIRCLE • ITHACA, NEW YORK

COMPENSATION FOR NONLINEAR EFFECTS DUE TO
HIGH HEAT FLUX IN THIN-FILM THERMOMETRY

by

J. W. Reece & R. W. Hale

TAR-TR 6601


June 1966

Submitted to

George C. Marshall Space Flight Center
Huntsville, Alabama

In partial fulfillment of Contract No. NAS8-20202

Approved by:

A handwritten signature in cursive script, reading "Alfred Ritter", is written over a horizontal line.

Alfred Ritter
President

ABSTRACT

N67-13131

A program of theoretical and experimental research has been carried out to devise practical means for compensating the electrical output of thin-film resistance thermometers for deviations from ideal performance that result when these gages are used to measure large heat transfer rates. These deviations have their source in an increase in the surface temperature of the gage of a sufficient magnitude to affect the materials properties — the thermal conductivity and thermal diffusivity of the substrate material, and the thermal coefficient of resistivity of the resistance element. It is shown that these temperature sensitive effects can be combined mathematically in a single correction factor and applied as an operation on the gage output. In practice this means that the gage output voltage is subjected to electrical compensation before it is introduced as the input to a conventional heat transfer analog unit.

Recent data on the pertinent materials properties have been used to evaluate the coefficients involved in the correction factors. Two different types of compensator network were then designed and built. Experimental apparatus was also built and operated to demonstrate that in either case the required operation was performed correctly.

The compensator units as well as the procedure for incorporating them into the operation of an analog unit are described in full.

A correction chart is also supplied, by the use of which uncompensated heat flux measurements can be corrected for the temperature-sensitive effects. However, the application of this chart is restricted to cases for which the applied heat flux is approximately constant.

Author

TABLE OF CONTENTS

INTRODUCTION	1
SECTION ONE - THEORETICAL FORMULATION OF COMPENSATION METHOD	
1.1 Solution of Nonlinear Diffusion Equation	3
1.2 Equation for Compensation of Sensor Output	9
SECTION TWO - NETWORK DEVELOPMENT FOR ON-LINE COMPENSATION	
2.1 Required Compensator Performance	12
2.2 PSQ Network	15
2.3 Varistor Network	17
SECTION THREE - EXPERIMENTAL VERIFICATION	23
SECTION FOUR - OPERATION IN CONJUNCTION WITH ANALOG UNIT	31
SECTION FIVE - CORRECTION OF UNCOMPENSATED HEAT FLUX MEASUREMENTS	
5.1 General Solution	35
5.2 Correction Under Constant Heat Flux Conditions	36
CONCLUSIONS AND RECOMMENDATIONS	39
REFERENCES	40
APPENDIX A - VARIATION OF PROPERTIES OF THIN-FILM SENSOR MATERIALS WITH TEMPERATURE	
A.1 General	41
A.2 Physical Properties of #7740 Pyrex	41
A.3 Properties of the Platinum Thin-Film Resistance Element	42

LIST OF PRINCIPAL SYMBOLS

a	constant defined in Eq. (9)
A	gain of scaling amplifier
b	constant defined in Eq. (5)
B	ratio e_i/\mathcal{T}_i
c	constant defined in Eq. (12) ; also, specific heat of substrate material
e	voltage
e_c	output voltage of compensator
e_i	input voltage to compensator
e_i	input voltage to compensator at design temperature limit
e_q	output voltage of analog network
i	current
k	thermal conductivity of substrate material
K	thermal diffusivity of substrate material
K_c	attenuation factor of compensator network at zero voltage
K_N	constant relating T_i and ΔV_g , Eq. (18)
q	heat flux
q_c	corrected heat flux
q_u	uncorrected heat flux
R	resistance
t	time
T	temperature increment from ambient conditions

T_i	indicated surface temperature rise, Eq. (14)
\mathcal{T}_i	design indicated surface temperature limit
T_w	surface temperature rise
y	distance below surface
β	$\sqrt{k\rho c}$
δ	parameter introduced in Eq. (30)
ΔR_g	resistance change of thin-film gage
ΔV_g	voltage change across thin-film gage
ϵ	λ/\mathcal{T}_i
θ	transformed temperature, Eq. (2)
$\theta_w^{(o)}$	transformed surface temperature rise for constant diffusivity
λ	parameter introduced in Eq. (17)
ρ	density of substrate material
Φ	initial tangent to R-T curve of thin-film gage
$()_o$	subscript affixed to k , K or β to denote value at room temperature

INTRODUCTION

The technique of thin-film resistance thermometry has found extensive application in obtaining heat transfer measurements in shock tubes, shock tunnels and other short-duration flow devices. Transient heating conditions are created in the operation of these devices, and it is a distinct advantage of this test technique that very large heat flux can be produced and measured under non-destructive conditions. The use of the thin-film resistance thermometer as a calorimetric gage has been found to be intrinsically suited to this short-duration mode of testing.

It has been found however that if the heat flux is high enough, even for the very brief times of exposure typical of short-duration test facilities, the surface temperature of a thin-film gage may rise into a range where the temperature dependence of the gage parameters cannot be neglected. Research into this problem began several years ago, starting at Cornell Aeronautical Laboratory with the early work performed by L. M. Somers¹ among others, and more recently by L. Bogdan². R. Hartunian and R. Varwig³ carried out a theoretical and experimental program at Aerospace Corporation, and, quite recently, Z. A. Walenta⁴ reported some further findings at UTIAS. The results of the first stage of the present research program have been reported by Reece⁵, and have led to an enhancement of the theory that forms the basis for handling the temperature-dependent effects. In addition, a survey of experimental data defining the temperature dependence of the materials properties was made. Guided partly by theoretical considerations, applicable data were then deduced from this survey. The highlights of these findings are carried over into the present work.

The usual method of fabricating thin-film resistance thermometers is to apply a thin strip of liquid bright platinum printed circuit paint (Hanovia 05-X) to the surface of a Pyrex button and then firing it in order to deposit the platinum metal which forms the resistance element. We are therefore concerned here with the thermal characteristics of these particular materials. The basic parameters in question are the density, specific heat capacity and thermal conductivity of the Pyrex, and the temperature coefficient of resistivity of the deposited platinum film.

The historical basis for the correction factor that has been deduced to account for temperature effects is found in the well-known textbook on heat conduction by Carslaw and Jaeger⁶. To account for temperature-dependent thermal conductivity, a transformed temperature is defined for which the customarily assumed linear form of the diffusion equation applies. This is an attractive result since, by working with the transformed temperature, conventional data reduction methods may be retained. For example, the voltage equivalent of the transformed temperature is the required input to a conventional, linear electrical analog network for calculating heat flux.

The basis for a further correction was laid by Hartunian and Varwig, who used perturbation techniques to solve for the contribution of temperature-variable diffusivity to the correction factor referred to above. Unfortunately, through a numerical error they considerably underestimated the magnitude of this effect and thereby concluded that it was negligible. This correction was restored in its correct magnitude in Ref. 5, in which it was shown that the contribution of variable diffusivity, and that of variable temperature coefficient of resistivity as well, could be accounted for by adjusting the value of the constant coefficient in the correction factor. Walenta, while he accepted the (erroneous) findings of Ref. 3 on the insignificance of the diffusivity effect, is in agreement with us regarding the form of the correction factor and the inclusion of the effect of variable temperature coefficient of resistivity in it.

In the present work the theory for compensating the input signal to be furnished to an electrical analog is outlined. Then the design of compensating networks to correct automatically for the effects of the temperature-variable materials properties is described. Particular attention is given to delineating the mathematical relationships between the electrical circuitry and the associated problem in temperature and heat flux. Circuit design and operation are completely characterized and related in detail to operational practice and requirements. The resulting networks represent a considerable simplification over previous efforts in this direction^{4,7}.

In addition to this approach of accomplishing on-line data compensation, it is also possible to apply a correction later to the heat transfer data obtained by conventional means. The correction in this case is somewhat more approximate than in the case of on-line compensation. The theory and resulting correction chart for this effect are given in this report.

SECTION ONE
THEORETICAL FORMULATION OF COMPENSATION METHOD

1.1 Solution of Nonlinear Diffusion Equation

Consider one-dimensional heat conduction into a semi-infinite solid which is at a uniform initial temperature, and in which the thermal conductivity and specific heat are functions of temperature. The equation governing thermal diffusion is

$$\rho c(T) \frac{\partial T}{\partial t} = \frac{\partial}{\partial y} \left[k(T) \frac{\partial T}{\partial y} \right] \quad (1)$$

This equation is taken to apply to the thin-film resistance thermometer*.

If the transformed temperature

$$\theta = \frac{1}{k_0} \int_0^T k \, dT \quad (2)$$

is introduced⁶ and the transformation applied to Eq. (1), the result is

$$\frac{\partial \theta}{\partial t} - K(\theta) \frac{\partial^2 \theta}{\partial y^2} = 0 \quad (3)$$

Eq. (3) provides the basis for solving the heat flux in terms of surface temperature history when taken in conjunction with the boundary condition,

$$q = -k_0 \left. \frac{\partial \theta}{\partial y} \right|_w \quad (4)$$

where the subscript w refers to conditions at the surface, $y = 0$.

Information regarding the properties of the materials used in thin-film thermometry is summarized in Appendix A. The results are shown plotted in Figs. 1-6. As seen from Fig. 2 the thermal conductivity varies linearly with temperature,

$$k = k_0(1 + bT) \quad (5)$$

* Two-dimensional effects on the performance of thin-film sensors are evaluated in Ref. 12.

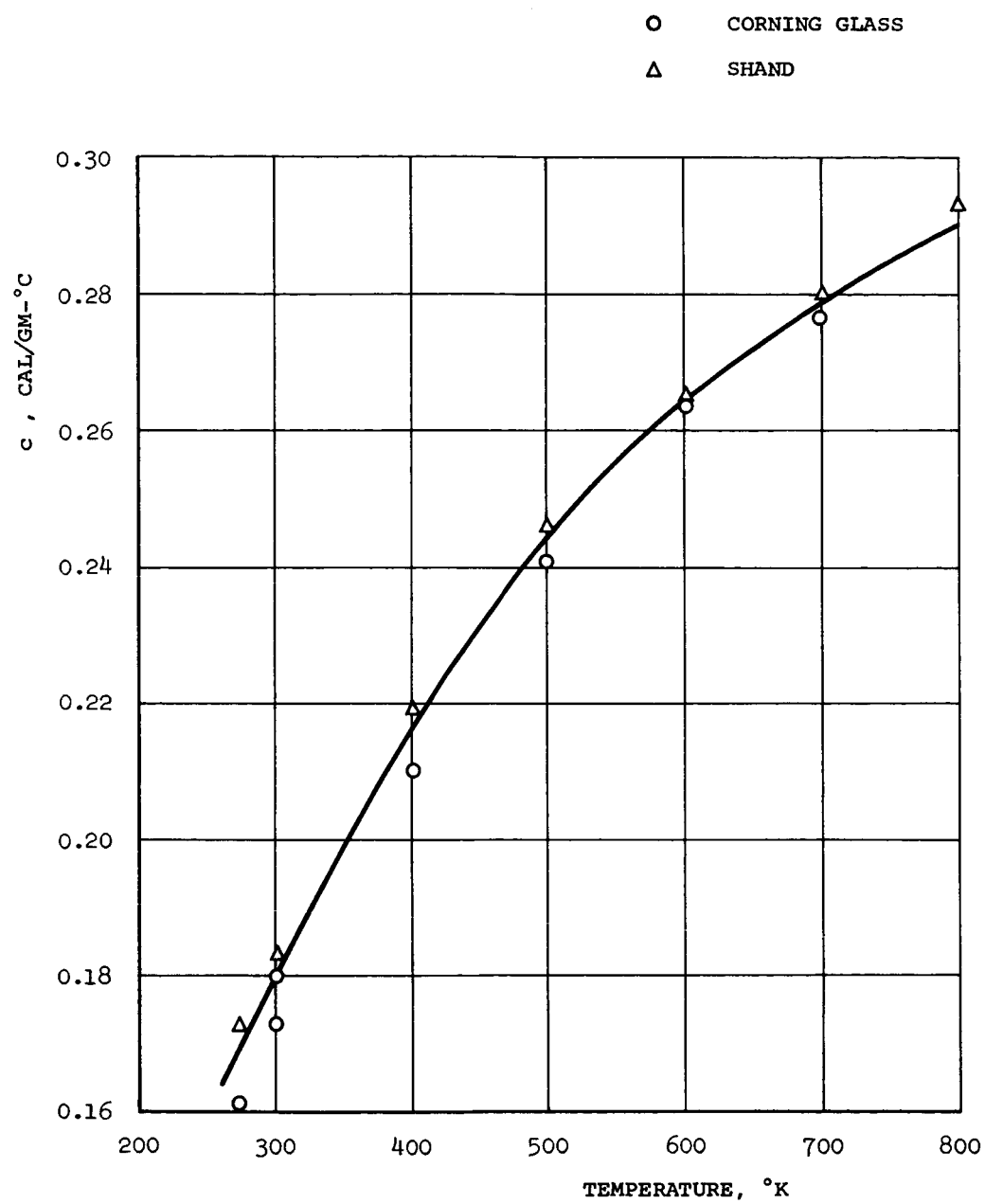


Figure 1. Specific Heat of #7740 Pyrex

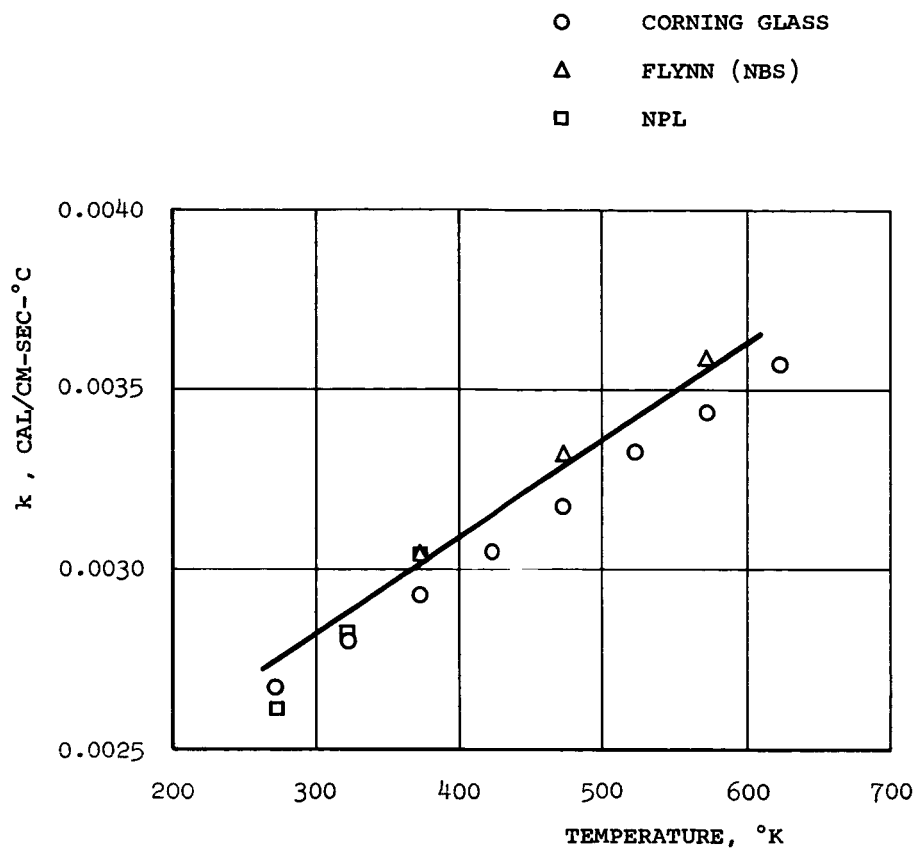


Figure 2. Thermal Conductivity of #7740 Pyrex

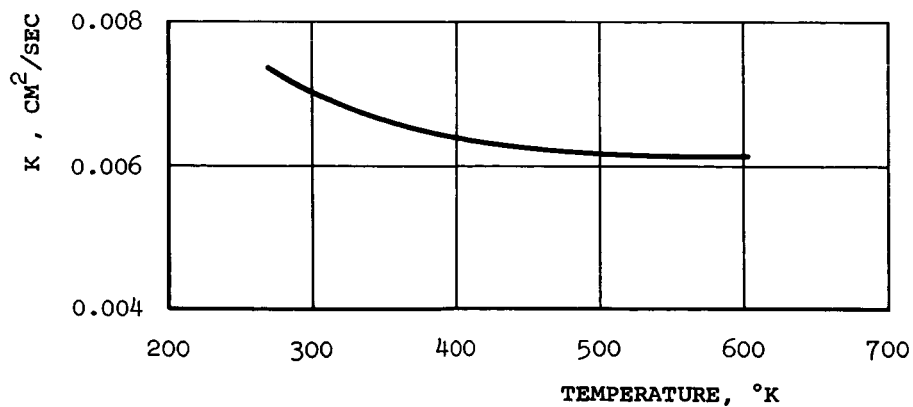


Figure 3. Thermal Diffusivity of #7740 Pyrex from Faired Data of Figs. 1 and 2

- Δ SOMERS¹
- \circ BOGDAN²
- \square HARTUNIAN³
- \triangleleft WALENTA⁴

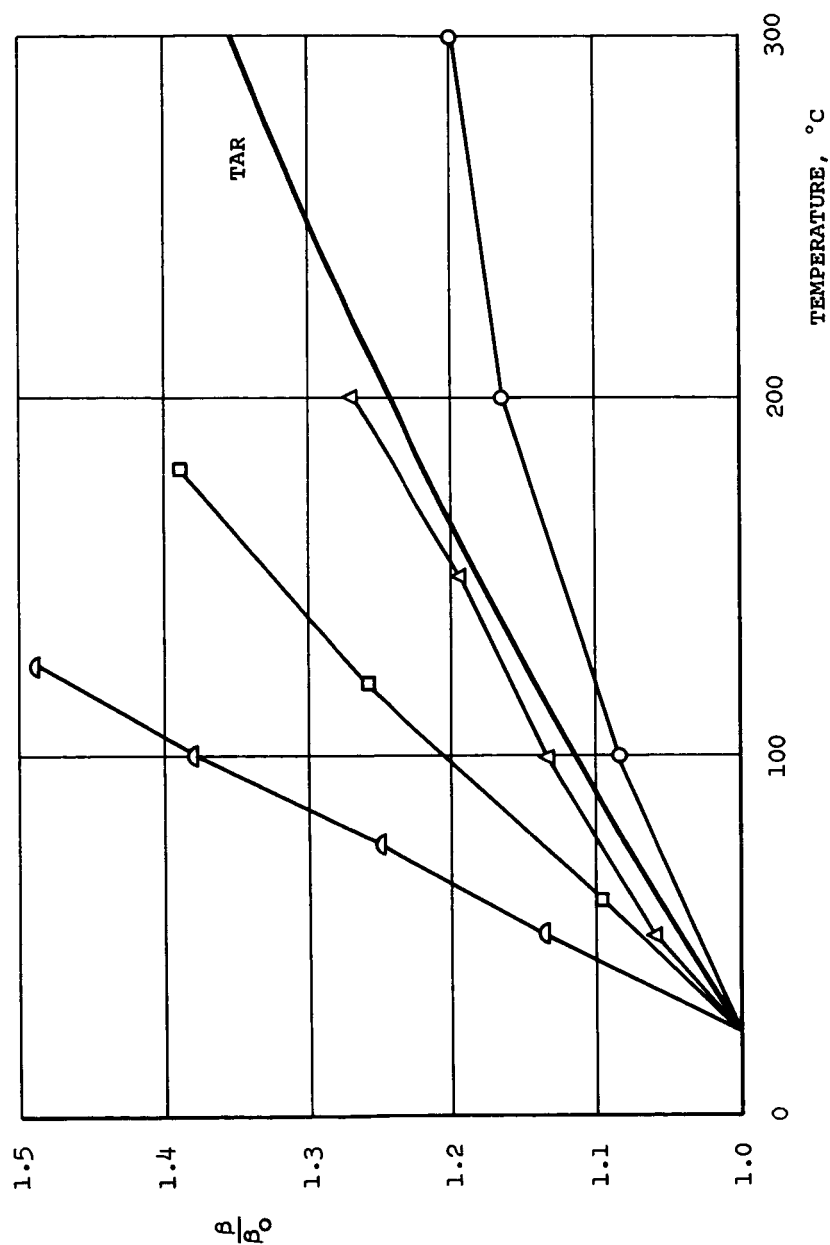


Figure 4. Temperature Dependence of β for #7740 Pyrex, Data Corrected for Nonlinear Variation of Thin-Film Resistance with Temperature

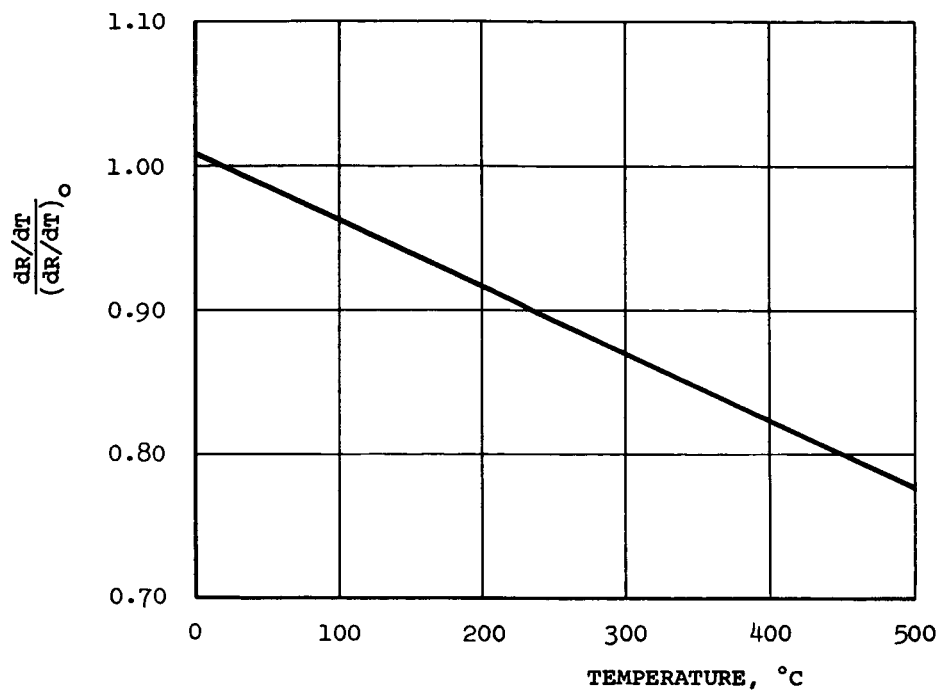


Figure 5. Variation of Thin Film Sensitivity with Temperature

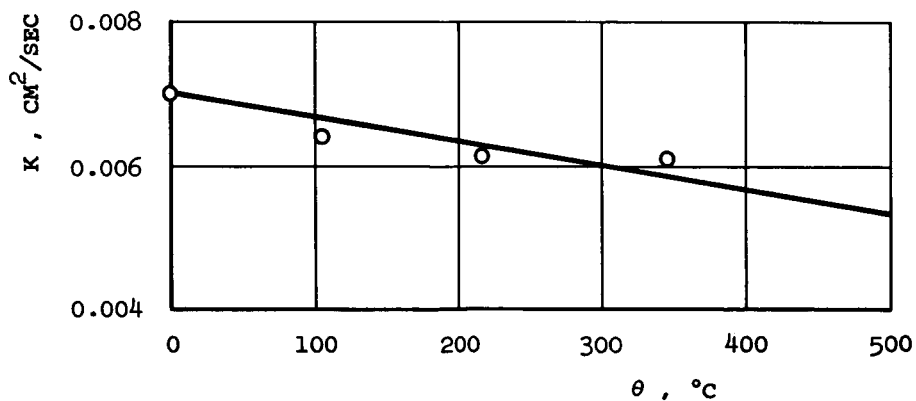


Figure 6. Thermal Diffusivity of Pyrex Versus Transformed Temperature Above Ambient

When this is substituted in Eq. (2) , the following simple relation between θ and T is obtained:

$$\theta = T(1 + \frac{1}{2}bT) \quad (6)$$

The quantity $(1 + \frac{1}{2}bT)$ may be thought of as a correction factor. Hartunian and Varwig used perturbation techniques to solve Eq. (3) and obtain a first-order correction for temperature-variable diffusivity. It was subsequently shown by Reece in Ref. 5 how the correction for $K(T)$ may be effected simply by making a change in the value of the coefficient appearing in the correction factor. The basis for this will now be explained briefly.

Consider that, to the zeroth order, the diffusivity is a constant, K_0 . Then the zeroth order form of Eq. (3) is

$$\frac{\partial \theta^{(0)}}{\partial t} - K_0 \frac{\partial^2 \theta^{(0)}}{\partial y^2} = 0 \quad (7)$$

This is the form of equation solved by the heat transfer analog networks used in thin-film thermometry¹³. For step-function heat input, of a magnitude $q = q_0$, the solution given by the zeroth-order system of equations, Eqs. (4) and (7) , provides the following well known equation applying to conditions at the surface:

$$\theta_w^{(0)} = 2 \frac{q_0}{k_0} \sqrt{\frac{K_0 t}{\pi}} \quad (8)$$

Let the diffusivity now be thought of as being given, to the first order, by the sum of a constant term K_0 and a perturbation quantity $K^{(1)}$. As a matter of convenience the perturbation term is assumed in the form $K^{(1)} = aK_0\theta^{(0)}$. That is, we take the diffusivity to be approximated by the equation,

$$K = K_0(1 + a\theta) \quad (9)$$

and determine the magnitude of a from the slope of the plot of K vs θ , Fig. 6 .

The perturbation method used by Hartunian and Varwig yields a first-order equation along with the zeroth-order equation, Eq. (7) . The solution of the first-order equation is given in Ref. 3 , and involves as a parameter the slope

a introduced in Eq. (9) . This result, when taken together with Eq. (8) , leads to the formulation of the correction factor applicable to surface temperature,

$$\theta_w^{(o)} = T_w \left[1 + \left(\frac{1}{2} b - \frac{\pi}{16} a \right) T_w \right] \quad (10)$$

as was detailed by Reece in Ref. 5 . The significance of this result is that any computing system capable of solving the linear diffusion equation, of which Eq. (7) is an example, to obtain heat flux as a function of surface temperature history, can still be used to solve the present problem involving temperature-variable materials properties, provided only that the input variable is transformed according to Eq. (10), namely, replacing T_w by $\theta_w^{(o)}$ as input quantity to the computing system. The electrical analog network that is described in a subsequent section of this report is an example of such a computing system.

Terms of the order of abT_w^2 , $a^2T_w^2$ and higher have been omitted from Eq. (10) on the basis of being small compared to unity. This is an excellent approximation here because a is relatively small and because no term in $b^2T_w^2$, which would otherwise be dominant among the higher-ordered terms, occurs. In any event it would be inconsistent to carry along the higher-order terms, since a linear approximation is being used to fit the curve of Fig. 6 . The coefficient $\pi/16$ occurring in Eq. (10) is that which has been calculated for the specific case of constant heat transfer rate. Evidence was given in Ref. 5 , however, that the numerical value of this coefficient is insensitive to the heat flux history.

1.2 Equation for Compensation of Sensor Output

A thin-film resistance thermometer is a passive circuit element and requires an external source of energization. A basic network for this was shown in Ref. 5 . It is generally possible to choose the circuit constants so that the output voltage signal is directly proportional to the resistance change of the sensor:

$$\Delta V_g = K_R \Delta R_g \quad (11)$$

where K_R is a constant of proportionality determined by the circuit parameters. Governed by Eq. (51) , see Appendix, the resistance change of the platinum-film element is a nonlinear function of temperature, namely,

$$\Delta R_g = \phi T_w (1 - cT_w) \quad (12)$$

in which ϕ is the initial resistance-temperature slope of the gage as

determined from the standard low temperature calibration, and c is a constant whose origin is in Eq. (51) ; in centigrade units, $c = 2.33 \times 10^{-4} (^{\circ}\text{C}^{-1})$.

Eq. (12) has to be inverted to solve for T_w in terms of ΔR_g with the result,

$$T_w = \frac{\Delta R_g}{\phi} \left[1 + \frac{c\Delta R_g}{\phi} + \dots \right] \quad (13)$$

We suppose that the same data that were used to provide Eq. (51) would also have been fit by a straight line if the data were plotted as dT/dR vs R rather than dR/dT vs T . Consistent with this observation, we have refrained from including higher-order terms in Eq. (13) .

The quantity $\Delta R_g/\phi$ appearing in Eq. (13) is the indicated surface temperature, defined by

$$T_i \equiv \frac{\Delta R_g}{\phi} \quad (14)$$

and so Eq. (13) becomes

$$T_w = T_i (1 + cT_i) \quad (15)$$

With this, Eq. (10) now provides

$$\theta_w^{(o)} = T_i \left[1 + \left(\frac{1}{2}b - \frac{\pi}{16} a + c \right) T_i + 2c \left(\frac{1}{2}b - \frac{\pi}{16} a \right) T_i^2 \right] \quad (16)$$

which is shown plotted in Fig. 7 . A straight-line approximation has been made to this curve:

$$\theta_w^{(o)} = (1 + \lambda T_i / \mathcal{T}_i) T_i \quad (17)$$

in which \mathcal{T}_i is the design temperature limit. For present purposes this is taken to be 300°C (above ambient). The corresponding value of λ is $\lambda = 0.25$.

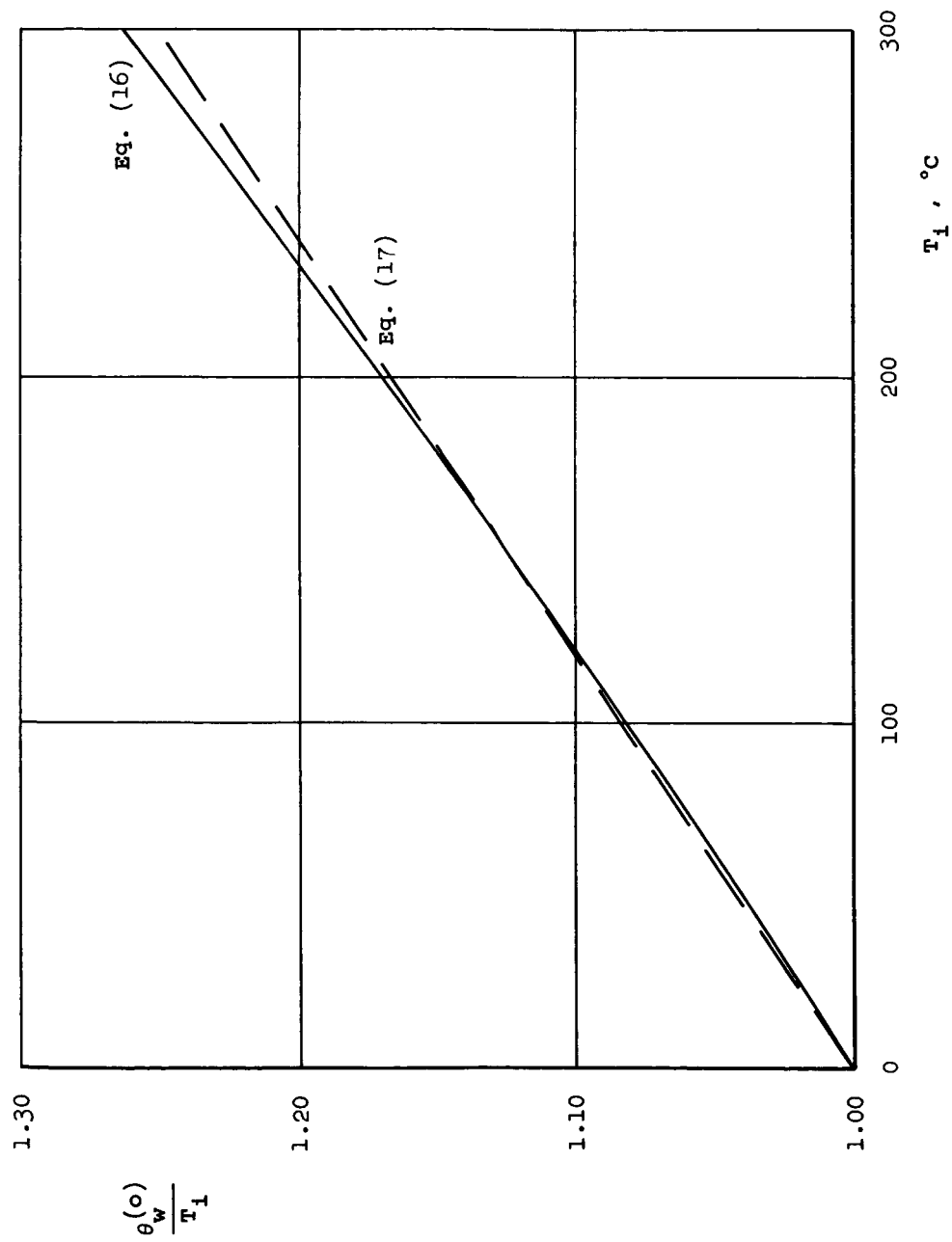


Figure 7. Required Compensation for Nonlinear Effects

SECTION TWO
NETWORK DEVELOPMENT FOR ON-LINE COMPENSATION

2.1 Required Compensator Performance

The material presented in this section relates to the common practice of using an electrical analog unit to provide on-line computation of heat flux. The main components of the system to be discussed are shown schematically in Fig. 8 . The transfer function at each stage is labeled in the appropriate box. We proceed to a discussion of the operations shown in Fig. 8 and of the relationships between the thermal and the electrical variables.

The foregoing analysis has defined the operation to be performed on T_i as that given by Eq. (17) . T_i is related to ΔV_g by $T_i = \Delta V_g / K_R \phi$, but for convenience we replace $K_R \phi$ by the symbol $1/K_N$ and write

$$T_i = K_N \Delta V_g \quad (18)$$

Then defining the gain of the scaling amplifier by $A \equiv e_i / \Delta V_g$, we obtain the relation between T_i and e_i as

$$T_i = \frac{K_N}{A} e_i \quad (19)$$

Evidently, from Eq. (19) , $T_i / \mathcal{T}_i = e_i / e_i$, which may now be substituted in Eq. (17) . It follows that the operation required to be performed by the electrical compensating network is

$$e_c = K_c (1 + \lambda e_i / e_i) e_i \quad (20)$$

where K_c is the initial (zero voltage) attenuation factor of the compensator.

The diagram given in Fig. 9 has been drawn to show the correspondence between the thermal quantities of the system and their electrical counterparts. The relation between T_i and e_i was given in Eq. (19) . The corresponding relation between $\theta_w^{(o)}$ and e_c may be found by substituting this in Eq. (17) and comparing the result with Eq. (20) , which gives

$$\theta_w^{(o)} = \frac{K_N}{AK_c} e_c \quad (21)$$

The design of the electrical analog network is based upon approximating

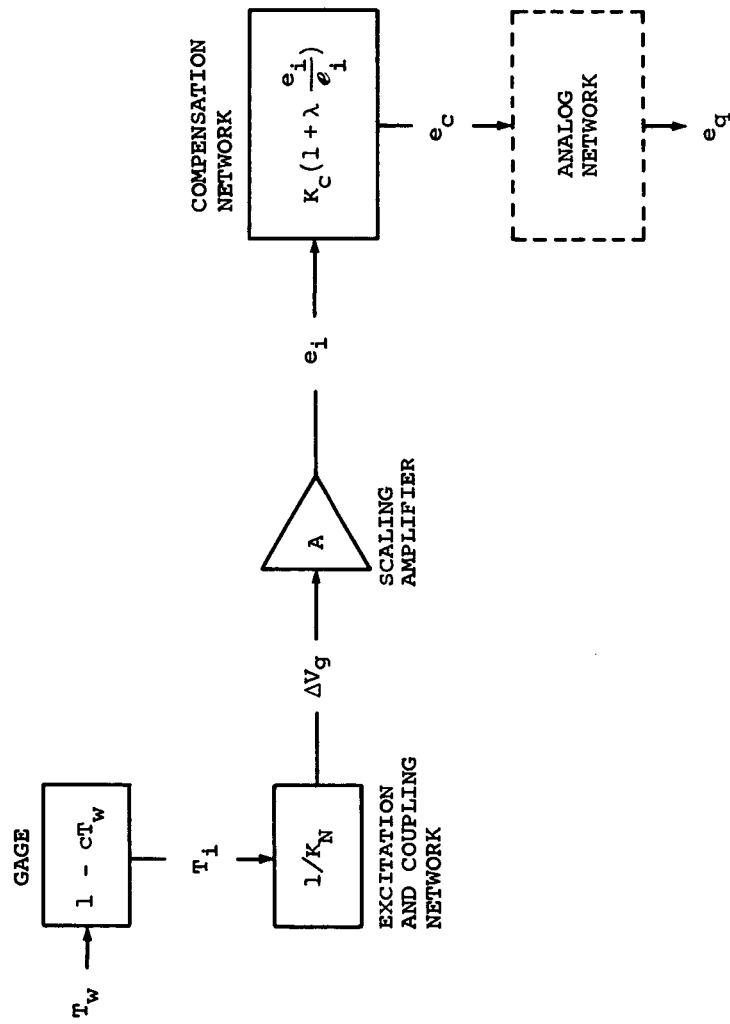


Figure 8. Schematic of Electrical Operations

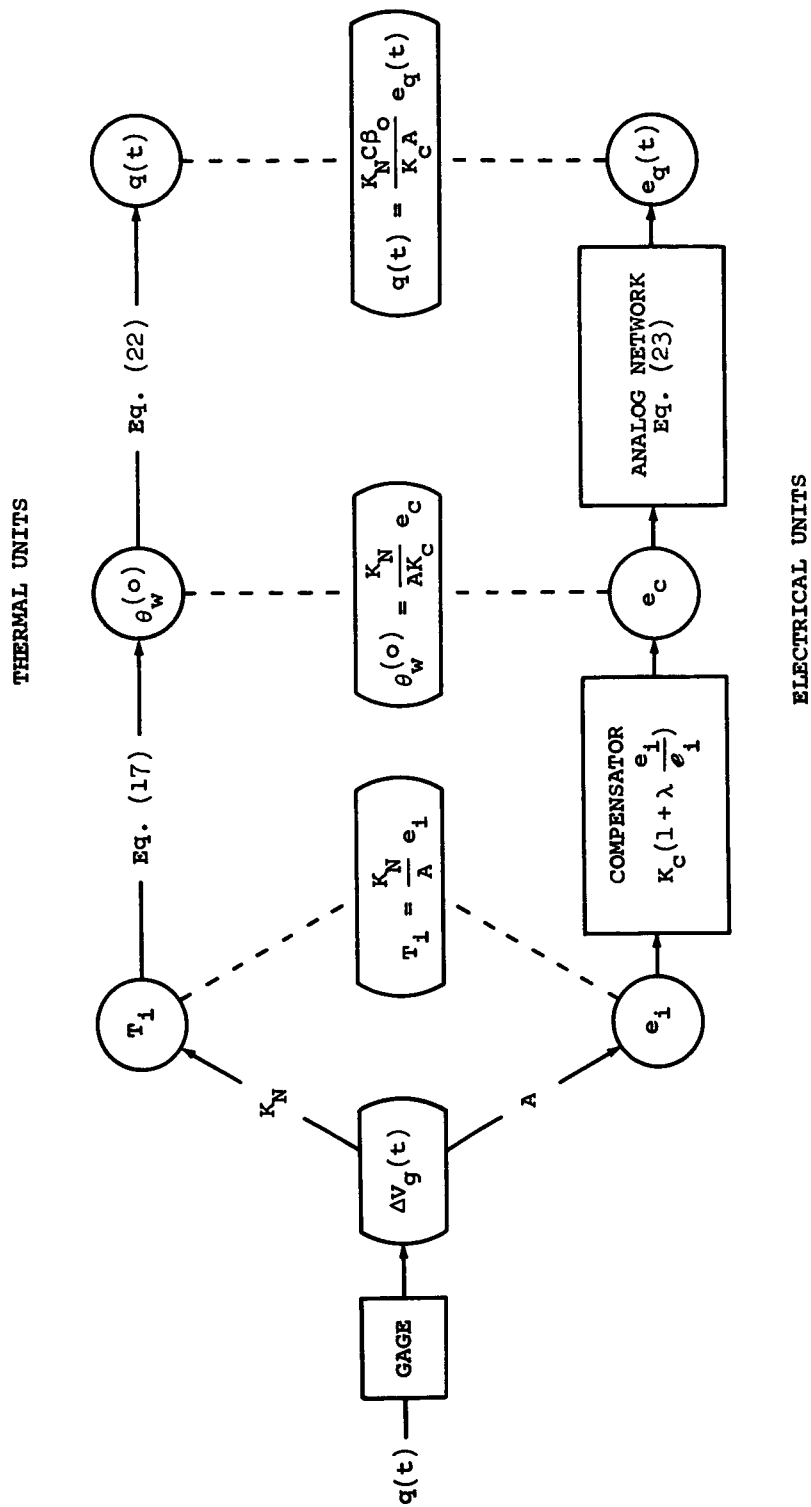


Figure 9. Correspondence Between Thermal and Electrical Quantities

the transfer function that relates the Laplace transforms of surface temperature history and heat flux to each other. This is described in detail in Ref. 13 . In Laplace transform terminology, the required operation is

$$\bar{q}(s) = \beta_o \sqrt{s} \bar{\theta}_w^{(o)}(s) \quad (22)$$

or, in terms of electrical units,

$$\bar{e}_q(s) = \frac{\sqrt{s}}{C} \bar{e}_c(s) \quad (23)$$

where C is a constant having units of angular frequency, and whose value is determined by the frequency scaling of the R-C network constituting the electrical analog. To obtain the relationship between the heat flux $q(t)$ and the analog output voltage $e_q(t)$, Eqs. (22), (23) and the Laplace transform of Eq. (21) are combined, then the inverse transform of the result yields

$$q(t) = \frac{K_N C \beta_o}{A K_c} e_q(t) \quad (24)$$

With regard to the design of the compensating network the parameters K_c and e_1 are at the disposition of the designer. Once these have been chosen, the required gain of the scaling amplifier is established, see Eq. (19), as

$$A = K_N \left[\frac{e_1}{\mathcal{F}_1} \right]_{\text{Design Limit}} \quad (25)$$

2.2 PSQ Network

The operation to be performed on e_1 may be carried out directly using commercially available equipment. Note that Eq. (20) is quadratic in e_1 . Consequently, a voltage-squaring component of equipment and a summing amplifier will provide means of mechanizing Eq. (20). This has in fact been done with the use of a Philbrick Model PSQ-P Quadratic Transconductor, a solid-state unit. This unit delivers to the summing point of an operational amplifier an output current proportional to the square of the input voltage:

$$i = 0.5 \left(\frac{e_1}{10v} \right)^2 \text{ ma} \quad (e_1 \geq 0) \quad (26)$$

The -P type transconductor does not conduct for negative input voltage.

Fig. 10 shows how the PSQ-P is combined with operational amplifier S to mechanize Eq. (20). Because the summing amplifier S has a very large open-loop gain (20,000 or greater) the normal practice of applying large negative feedback causes the summing point SP to be held at virtual ground potential. This facilitates the analysis of the system performance. Negligible current is drawn by the amplifier. The net current flowing into the summing point is given by

$$1 + \frac{e_i}{R_1} + \frac{e_c}{R_2} = 0 \quad (27)$$

which, with Eq. (26) may be used to solve for e_c ,

$$\begin{aligned} e_c &= -\frac{R_2}{R_1} e_i - 0.5 \times 10^{-3} R_2 \left(\frac{e_i}{10} \right)^2 \\ &= -\frac{R_2}{R_1} e_i \left(1 + 0.5 \times 10^{-4} R_1 \frac{e_i}{10} \right) \end{aligned} \quad (28)$$

The nominal working range for the transistorized components used in this network is 0-10 volts. Comparing Eq. (28) with Eq. (20), we note that for λ to be 0.25, R_1 must equal 5,000 ohms. Finally, for e_c to be 10 volts when e_i is 10 volts, R_2 must equal 4,000 ohms. The low voltage attenuation of this network is, therefore, $K_c = R_2/R_1 = 0.8$.

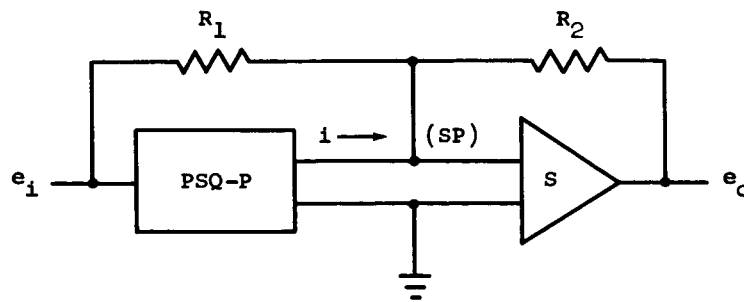


Figure 10

2.3 Varistor Network

An even simpler network may be devised to perform the corrective operation on e_i . This is essentially a voltage divider with a voltage-variable resistor, or varistor, as one of the elements. A design analysis of this network has been carried out and will be described in this section.

The varistor is characterized by a rapidly decreasing resistance with increasing applied voltage. Generally, however, its behavior is expressed in the form $i \sim e^n$, where i is the current through the varistor and e the applied voltage. The exponent n is usually fairly constant over its operating range and can be from 2 to 7 depending upon various factors in the manufacturing process. Varistors are made from silicon carbide which is mixed with a ceramic binder, molded in the desired shape, and fired at high temperatures. They are electrically stable, do not age if properly operated, and have essentially equal non-linear characteristics for both polarities. They exhibit a negative temperature coefficient of resistance of up to $-0.7\%/^{\circ}\text{C}$ for temperatures from $0-100^{\circ}\text{C}$, with the higher coefficients associated with higher values of n . Varistors also exhibit a small amount of capacitance, the equivalent circuit being a resistor and capacitor in parallel.

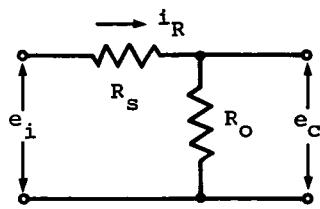
If a varistor is connected in series with a resistance, it is shown in Ref. 14 that the voltage drop across the resistance can be made proportional to a selected power of the input voltage by the proper selection of the varistor and series resistance. If we then combine this circuit with a simple dividing network, as shown in Fig. 11, we obtain a network which will generate the non-linear function given by Eq. (20). The use of this type of circuit was explored briefly in Ref. 7.

The relation between the input and output voltages can be written in the form

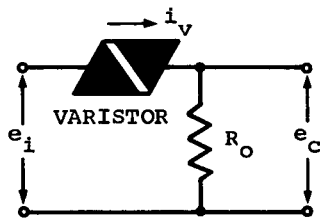
$$e_c = \frac{e_i}{1 + \frac{R_s}{R_o}} \left[1 + \frac{R_s i_v}{e_i} \right] \quad (29)$$

where i_v is the varistor current, and R_s and R_o the shunt and the series resistances, respectively. If R_{vo} is the zero or low voltage resistance of the varistor, then the network attenuation at low voltage, see Eq. (20), is given by

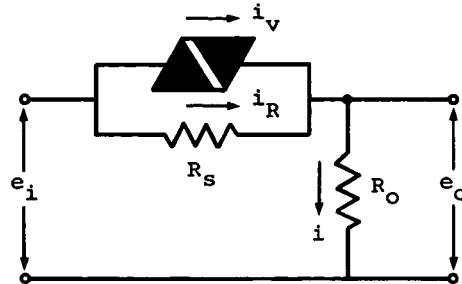
$$K_c = \frac{1 + \frac{R_s}{R_{vo}}}{1 + \frac{R_s}{R_o} + \frac{R_s}{R_{vo}}} = \frac{1 + \delta}{1 + \frac{R_s}{R_o}} \quad (30)$$



$$e_c = i_R R_o \sim e_i$$



$$e_c = i_v R_o \sim e_i^2$$



$$e_c = i R_o = i_R R_o + i_v R_o$$

Figure 11. Basis for Varistor Compensator Design

where

$$\delta \equiv \frac{\frac{R_s}{R_o} \frac{R_s}{R_{vo}}}{1 + \frac{R_s}{R_o} + \frac{R_s}{R_{vo}}}$$

Combining Eqs. (20) and (30) , we obtain the required variation in the dimensionless varistor voltage:

$$\frac{e_i - e_c}{e_i} = \frac{e_i / e_i}{1 + \frac{R_o}{R_s}} \left[\left(1 - \delta \frac{R_o}{R_s} \right) - (1 + \delta) \lambda \frac{R_o}{R_s} \frac{e_i}{e_i} \right] \quad (31)$$

Similarly, the dimensionless varistor current variation is found to be

$$\frac{R_s i_v}{e_i} = (1+\delta) \lambda \left(\frac{e_i}{e_i} \right)^2 + \delta \frac{e_i}{e_i} \quad (32)$$

as a result of combining Eqs. (20) , (29) and (30) . For any λ , R_o/R_s , and δ , the required relationship between the dimensionless varistor voltage and current is given by Eqs. (31) and (32) as e_i/e_i is varied from 0 to 1 . Upon matching a specific varistor characteristic to this curve, the values of e_i and R_s are then determined, and so R_o as well.

Since exact matching of the actual and desired varistor curves is impossible, it is desirable to work instead within a specified error on either side of the desired characteristic. Using Eq. (29) , one can find the error in the output voltage Δe_c as a function of the error in the dimensionless varistor current $\Delta(R_s i_v/e_i)$ for any fixed value of the input voltage e_i . Inverting this we get the expression

$$\frac{\Delta(R_s i_v/e_i)}{R_s i_v/e_i} = \left(1 + \frac{e_i/e_i}{R_s i_v/e_i} \right) \frac{\Delta e_c}{e_c} \quad (33)$$

which specifies the allowable error in the dimensionless varistor current for any given percent error in e_c which can be tolerated.

The varistor performance is defined by Eqs. (31) - (33) . Illustrated in Fig. 12 are bands for $\delta = 0.01, 0.03, \text{ and } 0.05$, where we have taken $\lambda = 0.25$, $\Delta e_c/e_c = 0.01$, $R_s/R_o = 1.0$, and e_i/e_i between 0.1 and 1.0 . Although δ is usually small, it is seen that variations in δ must be taken into account if accuracy on the order of 1% is desired. Correspondingly, the low voltage resistance of the varistor cannot be assumed infinite.

The varistor chosen for use in the compensator network was the VECO 063L4 . Although certain other varistors might display equally suitable non-linear performance, this one operates in a voltage and current range which is low enough to allow the use of a relatively inexpensive solid-state scaling amplifier. Since there is some variation in the performance of individual varistors, twenty-five of this type were purchased and tested. The measured characteristics curves fall between those of varistors #1 and #21 shown in Fig. 13 . The curve for varistor #3 is also shown since it and several others with virtually identical performance were ultimately selected for use in the network. All these curves apply to a d-c voltage source. To indicate the effect of varistor capacitance, measurements were made with varistor #1 using an oscillator at several selected frequencies. As shown in Fig. 13 , the effect is most pronounced at low voltage when the varistor resistance is high.

$$R_s/R_o = 1.0, \quad \lambda = 0.25, \quad \Delta e_c/e_c = 0.01$$

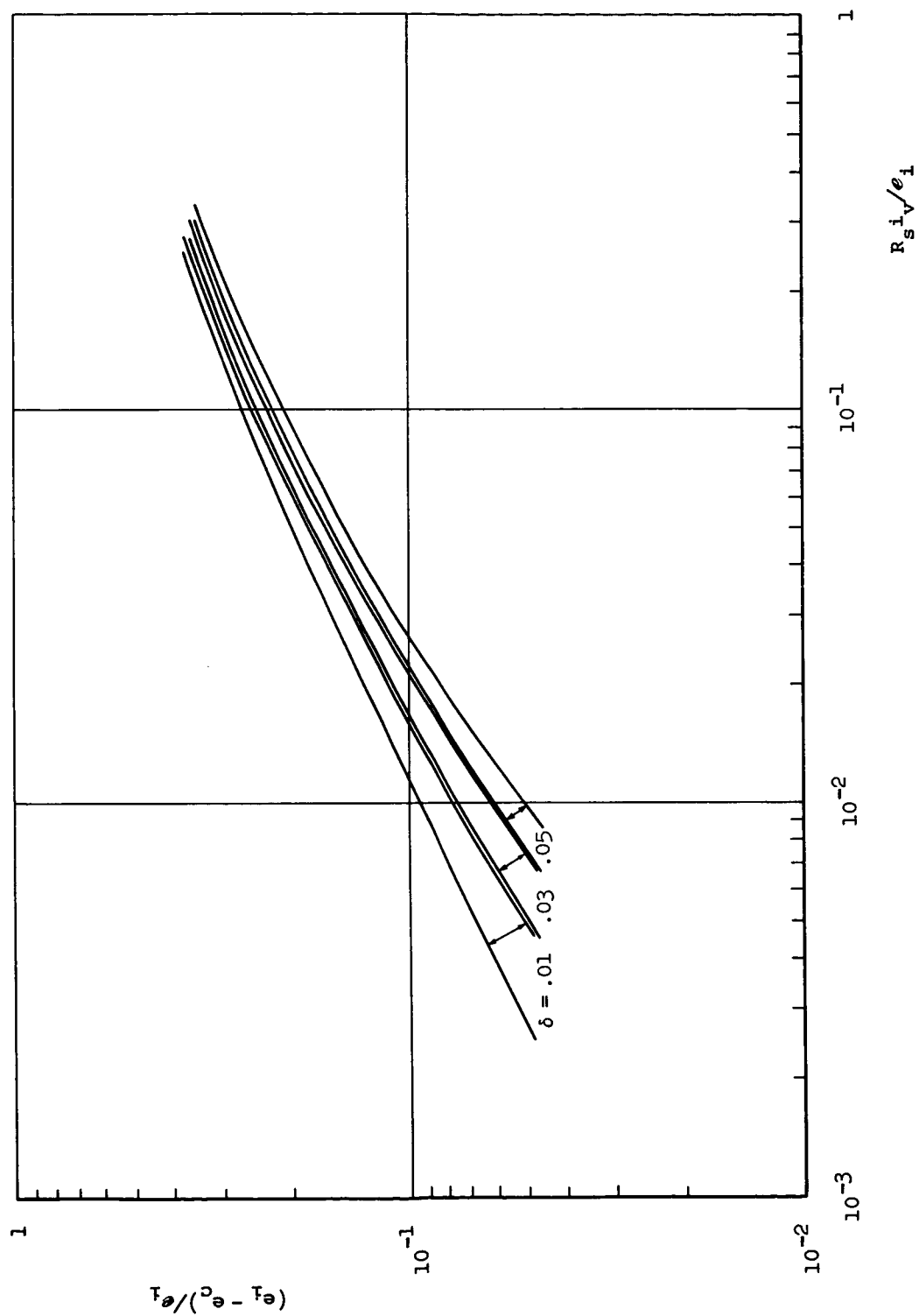


Figure 12. Required Varistor Performance

	VARISTOR	R_{VO}
—	# 1	191,000 ohms
- - -	# 3	129,000 ohms
- - -	#21	83,000 ohms

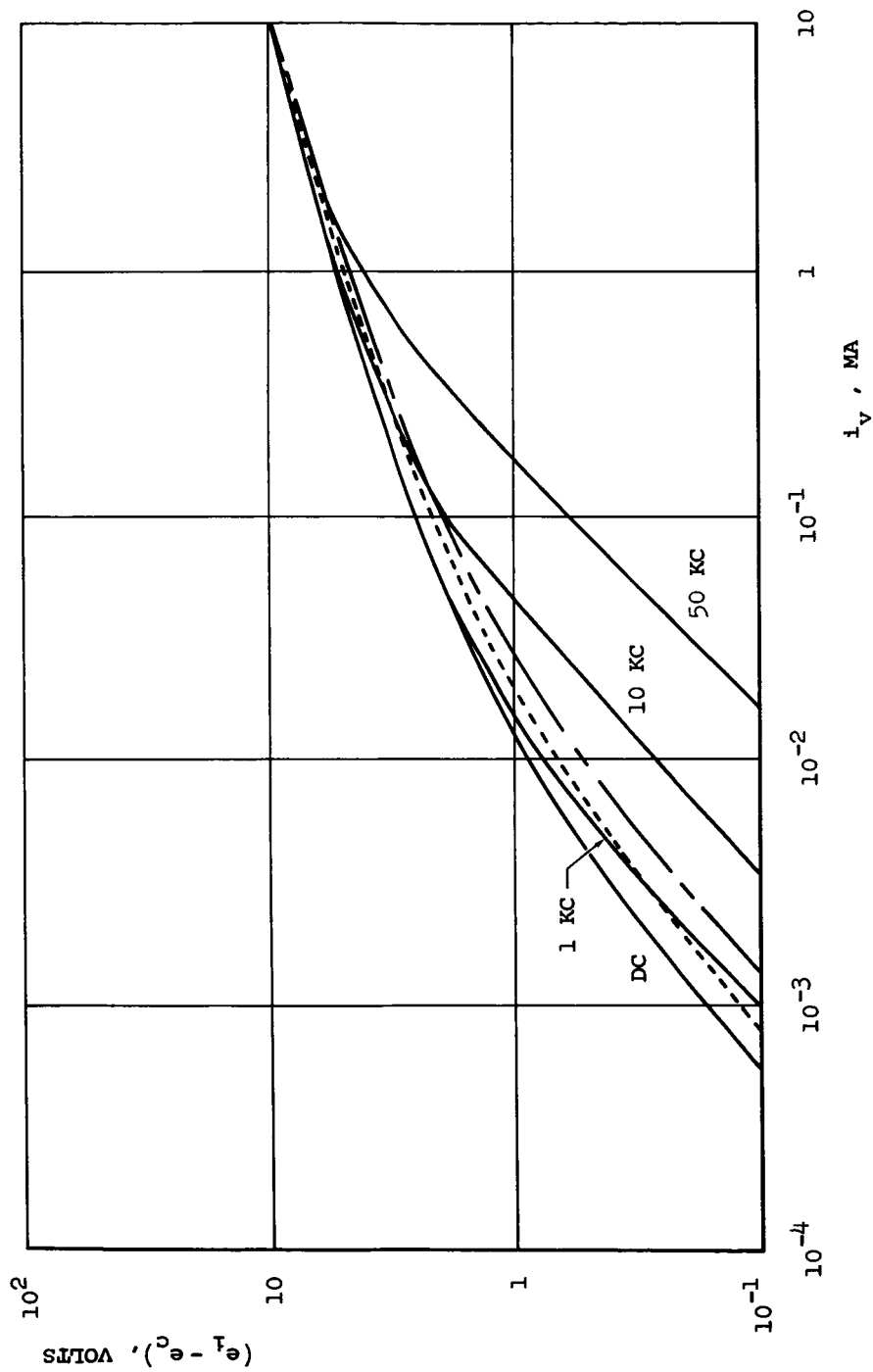


Figure 13. Measured Performance of VECO 063L4 Varistors

The procedure for matching individual varistor characteristic curves to the calculated bands defining the required performance is an iterative one since δ is not known a priori. The first step is to determine which value of R_s/R_o gives the best overall fit to the varistor curves. Values of 0.8, 1.0 and 1.2 were tried and $R_s/R_o = 1.0$ selected. Next, a value of δ must be chosen and the matching carried out by laying each varistor curve over the required performance band. For the scaling amplifier used, it was desirable to establish $e_i = 10$ volts. The associated limiting condition on the maximum of $(e_i - e_c)$ is determined by Eq. (31).

The matching process consists first of finding varistor curves which fit acceptably within the calculated band. To calculate R_s , only one matching point is required. This was taken to be at maximum voltage, or $e_i = e_i$, so that

$$R_s = \frac{(e_i - e_c)}{i_v} \left[\frac{R_s i_v / e_i}{(e_i - e_c) / e_i} \right]_{\text{Maximum}} \quad (34)$$

The quantities in the first fraction come directly from the varistor characteristic, while those in the second come from the required performance plot. Once R_s is found, δ can be calculated and compared with the assumed value. If there is significant disagreement, a new value must be chosen and the procedure repeated. Similarly, if matching becomes difficult with the value of R_s/R_o chosen, others should be used. To keep δ from increasing too rapidly during the iteration procedure, it was found helpful to pick varistors with as low a ratio of minimum to maximum resistance. The minimum resistance is simply the first fraction in Eq. (34) so that minimizing this ratio effectively minimizes R_s/R_{vo} and, in turn, δ . Some compromise was necessary, however, since varistors with the lowest values of this ratio generally had too large an exponent n for good matching.

We found that final adjustment of the parameters R_s , R_o and e_i could best be done by comparing the actual and desired performance using the varistor data directly and Eqs. (20) and (30). An initial value of e_i can be obtained from the ratio of the maximums of $(e_i - e_c)$ and $(e_i - e_c)/e_i$ which quantities were used in Eq. (34) to obtain R_s . First, e_i was rounded off to a convenient value; then $R_s = R_o$ was adjusted so as to yield the same maximum positive and negative errors in e_c as e_i/e_i varies from 0 to 1. In this way the error in the compensation at any voltage is held to a minimum.

These calculations were carried out for the set of varistors of which varistor #3 is typical. Optimum performance was found with $e_i = 10.0$ volts and $R_s = R_o = 8400$ ohms. The low voltage resistance of these varistors was measured to be from 120,000 to 130,000 ohms; therefore, $K_c = 0.516$ to 0.517 and $\delta = 0.031$ to 0.034 . The computed error in e_c was everywhere less than 1.3%.

SECTION THREE

EXPERIMENTAL VERIFICATION

Special attention has been given to provide means for demonstrating and comparing the operation of these compensating units under conditions simulating actual use. With this in mind, the necessary electronic circuitry has been designed and built. Experimental operations have been carried out, and the results recorded photographically.

The demonstrator unit consists of two interconnected chassis. The main function blocks, shown in Fig. 14, are a pulse generator, a parabola generator, the compensator, and an electrical analog network. Chassis #1 contains the varistor compensator along with all the other main function blocks; Chassis #2 contains the PSQ compensator and power supply, and a high input impedance coupling amplifier (follower) for the varistor compensator. Photographs of these chassis are given in Figs. 15 and 16.

The operation of the unit is based on the condition of a constant heat flux being applied suddenly to a thin-film resistance thermometer. The applied heat flux is therefore simulated by a rectangular voltage pulse. The demonstrator unit then provides, essentially, comparisons of conditions with and without the inclusion of a compensating network. In particular, the effect on the deduced heat flux is shown. The operation of the compensator units themselves, it should be remembered, does not require the heat flux to be constant.

The system is set up for a pulse duration of 25 msec. The limiting case of $T_1 = T_i = 300^\circ\text{C}$ above ambient at the end of the 25 msec test period is simulated. Consequently, the demonstrator unit as set up depicts conditions corresponding to the design limit of the compensators.

The wiring diagram of the network is shown in Fig. 17. The original pulse is generated by a mercury-wetted relay having its coil capacitively coupled to the energizing source, a 9 volt mercury cell. The parabola ($e_3 \sim \sqrt{t}$) is generated by using an analog network in the feedback loop of operational amplifier A-2. An important operation that the network is called on to perform is to simulate the high temperature effects by suitably modifying the normally parabolic output of A-2. The analysis of Section 5 provides the basis for this. To first order, what is called for is to subtract from the rectangular pulse e_1 a voltage proportional to \sqrt{t} . To do this identically, three operational amplifiers are required. We have chosen instead to approximate this operation with fewer amplifiers.

Two methods of generating the modified parabola were devised. In Mode 1 the output voltage e_3 of amplifier A-2 (refer to Fig. 14 for key to voltage notation) is fed back through a suitably chosen resistor to the input of A-2. Thus e_2 is the negative of the sum of e_1 and a fraction of e_3 , e_3 being

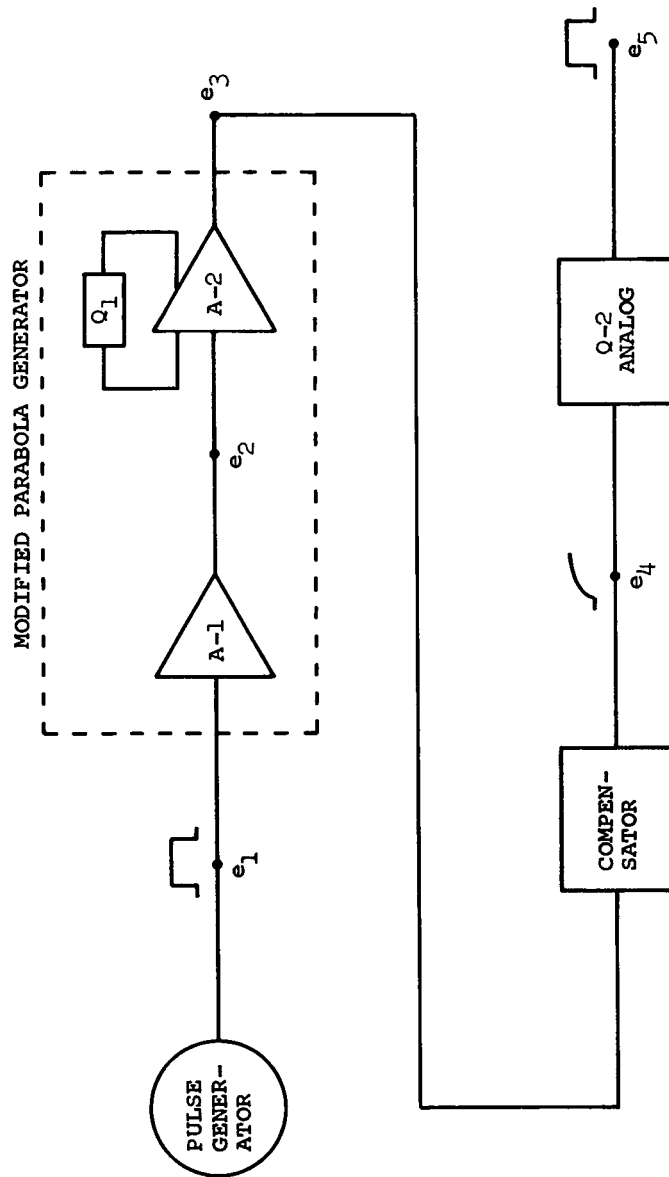


Figure 14. Block Diagram of Demonstrator Unit

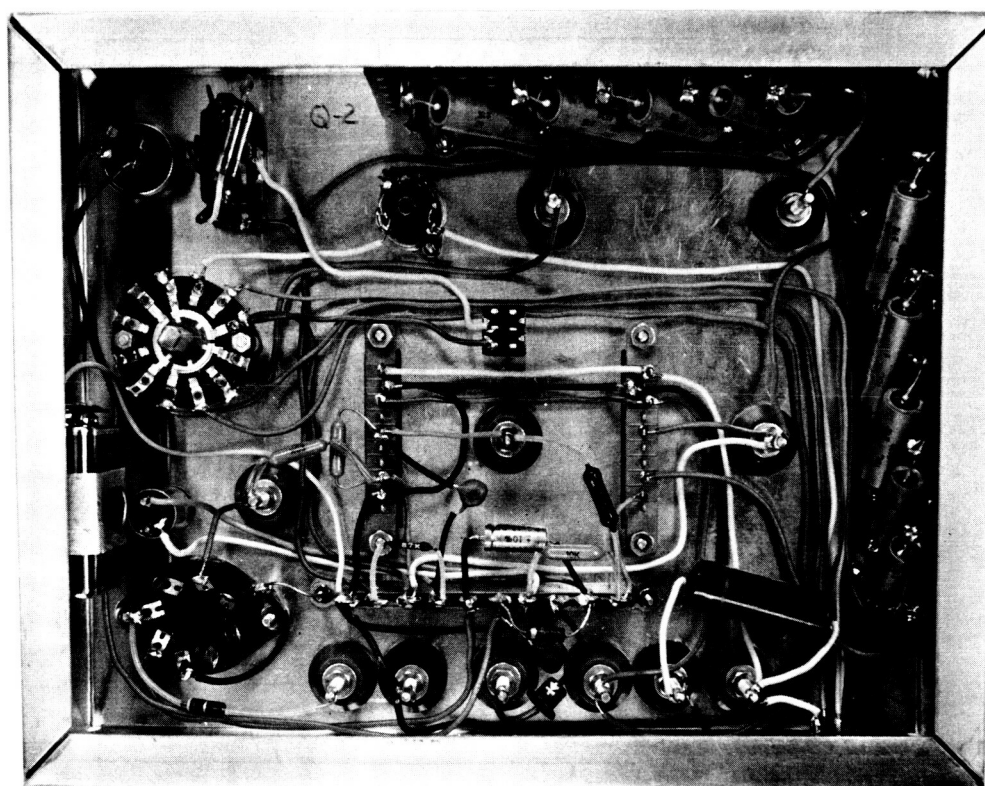
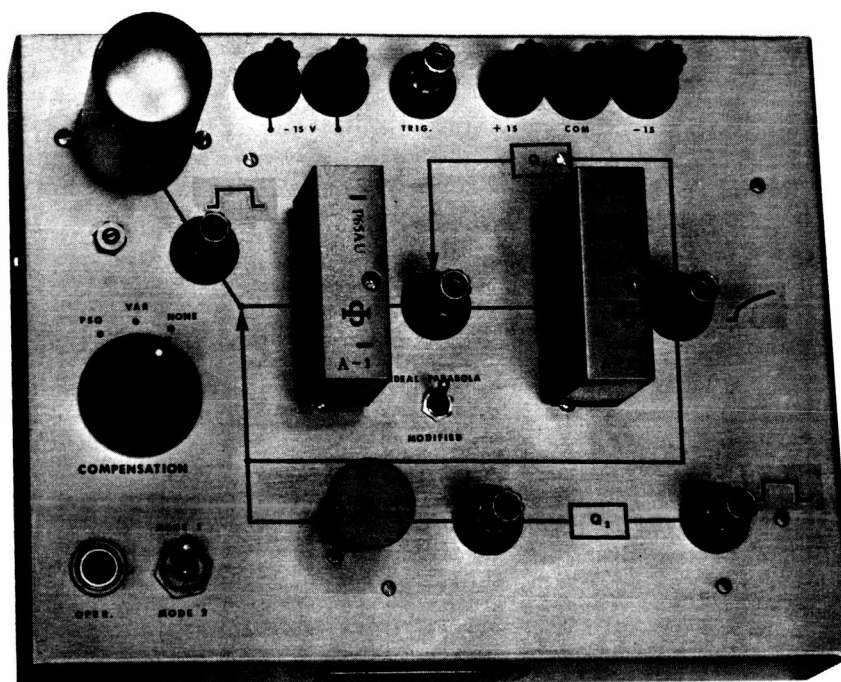


Figure 15. Demonstrator Unit - Chassis #1

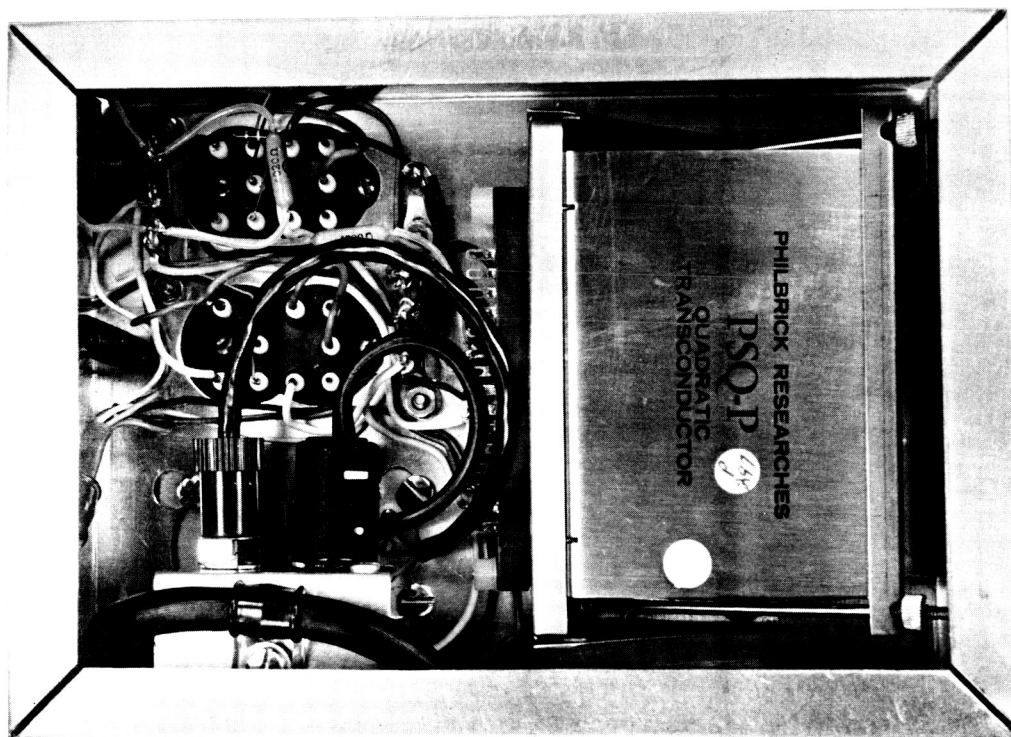
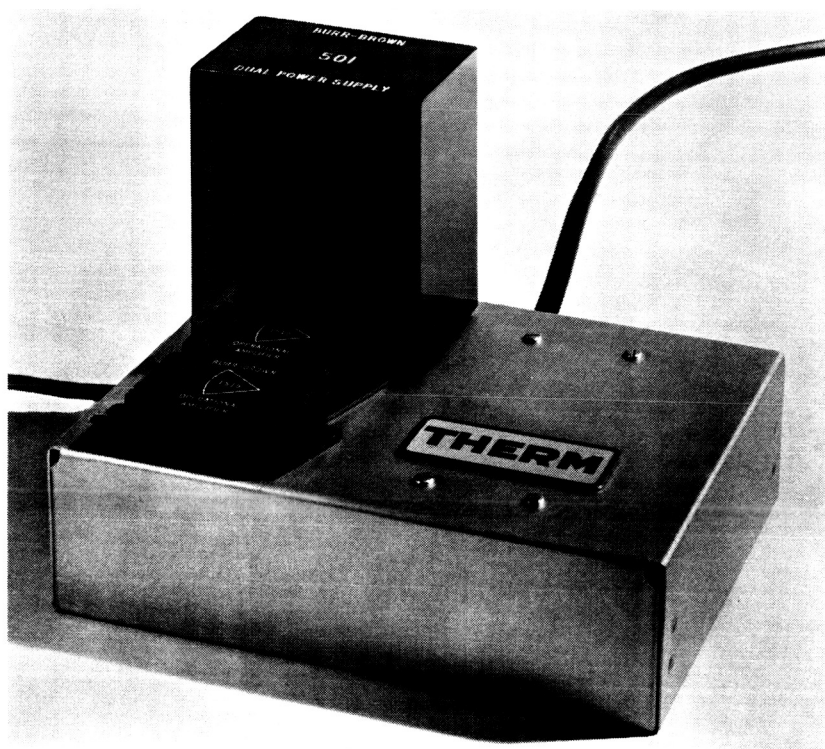


Figure 16. Demonstrator Unit - Chassis #2

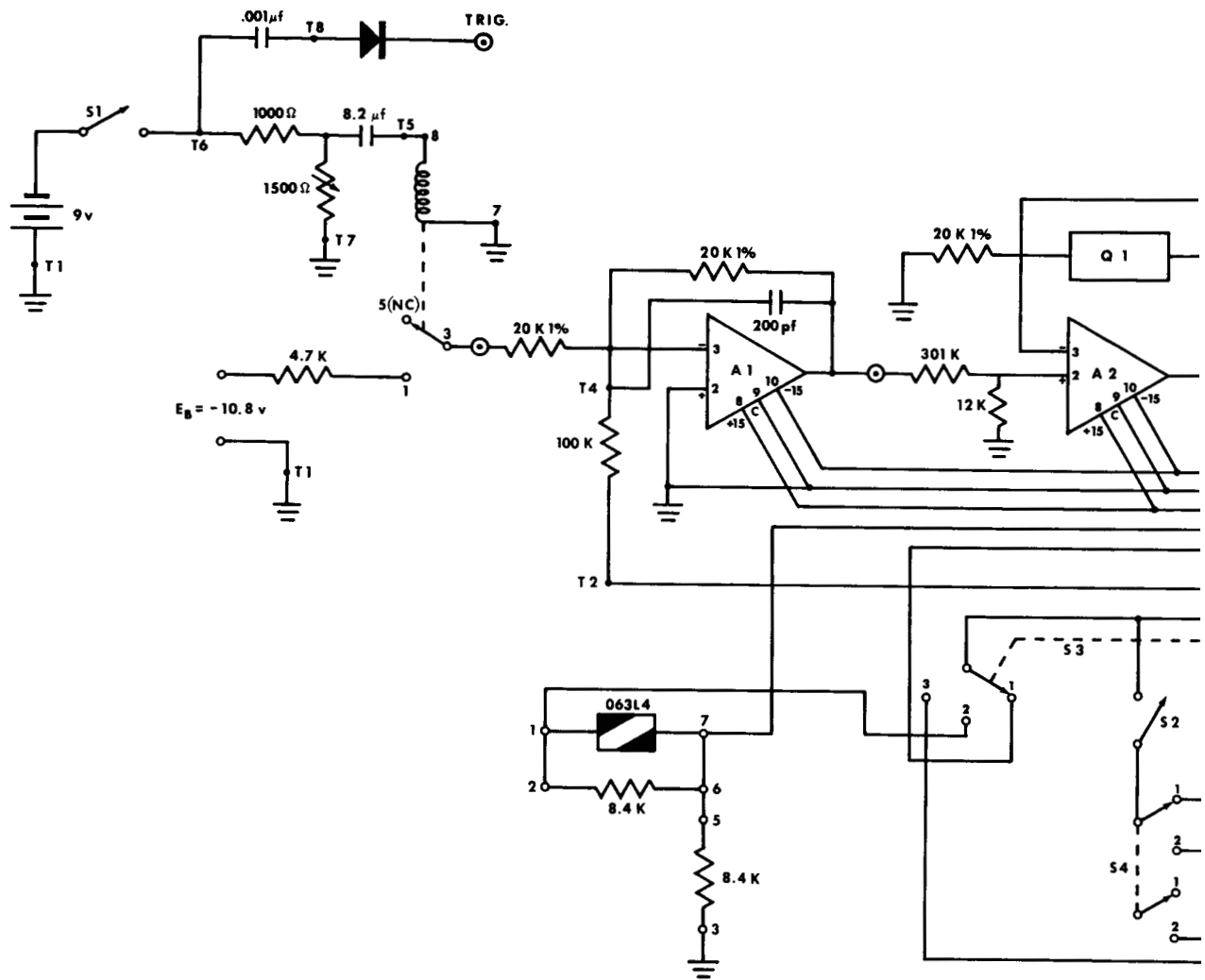


Figure 17. Wiring Diagram

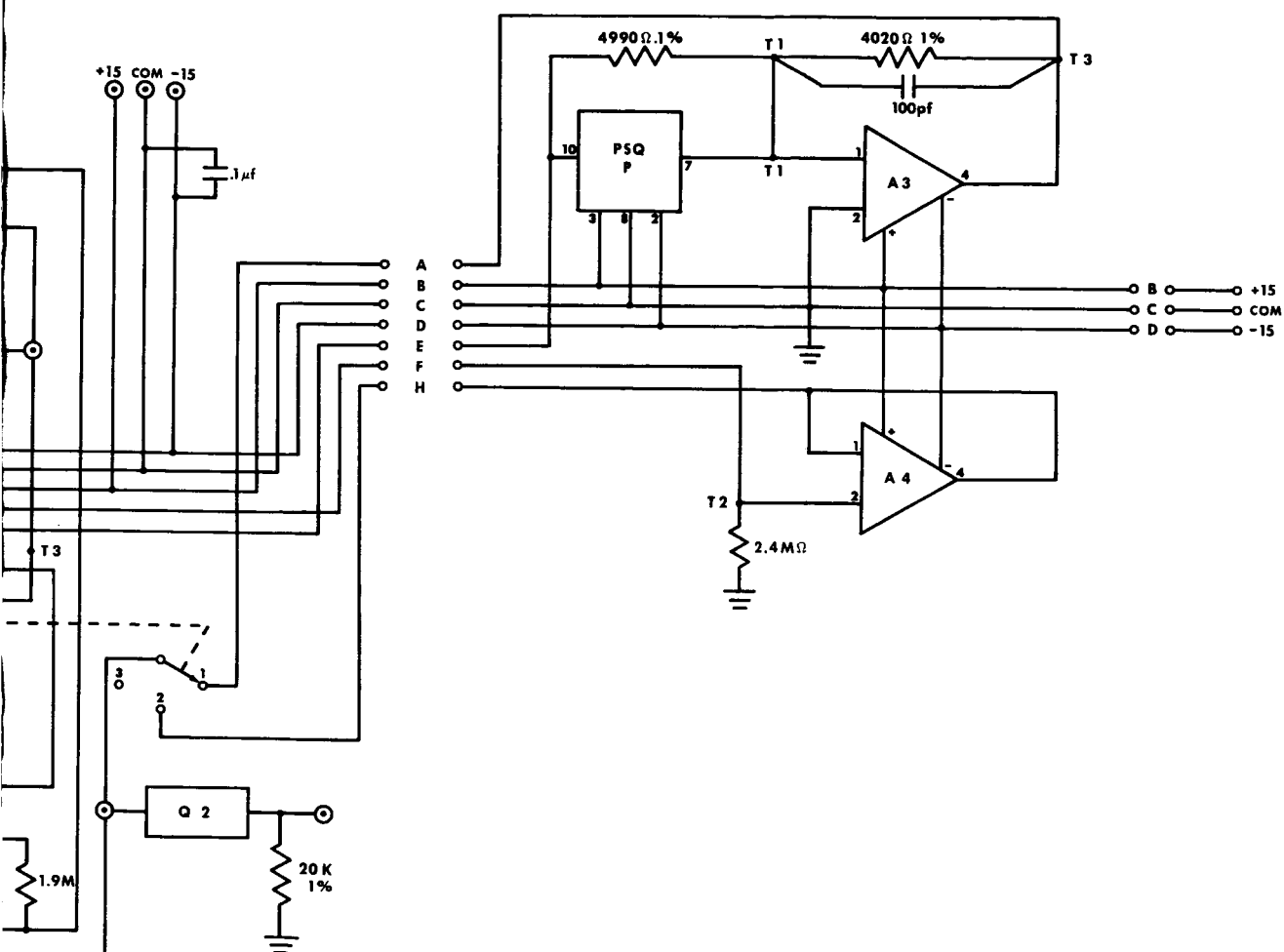


Diagram of Demonstrator Unit

27-2

opposite to e_1 in polarity. In Mode 2 a suitably chosen resistor is connected in parallel with the feedback loop of A-2 (which is the analog network Q-1). In this latter mode $e_2 = -e_1$ and a single amplifier, A-2, generates the modified parabola. The values of these respective feedback resistors were obtained by the substitution method using a resistance decade box. The output e_3 , representing the modified parabola, was compared to the corrected output e_4 provided by the PSQ compensator. The d-c supply voltage E_b and the decade box setting were adjusted to bring the maximums of e_3 and e_4 coincident at 10 volts, as was required in Section 2.2. A resistor of corresponding value was then installed.

Experimental results obtained with this demonstrator unit have been recorded by oscilloscope photography. The runs shown in Figs. 18a-g were made at a sweep rate of 5 msec/cm. This sweep timing and choice of test time reflects the frequency scaling of the electrical analog units employed.

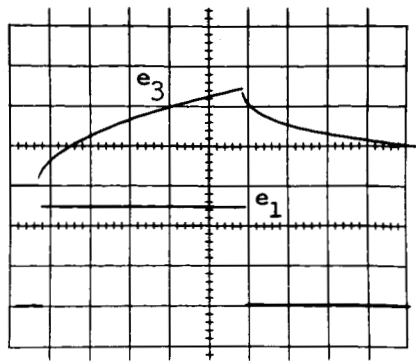
Fig. 18a shows the quality of the square-wave pulse and the parabola e_3 derived from it. Fig. 18b shows the same parabola $e_4 = e_3$ and the quality of the resulting output e_5 of the analog unit. The analog performance may be judged to be excellent, but its high frequency response capability should not be overestimated on the basis of Fig. 18b. This is because the parabola e_3 itself has a singularity (a small discontinuity) at $t = 0$ due to the limited high frequency response of Q-1, the analog network placed in feedback to A-2. This singularity tends to be compensated by the correlative response characteristic of Q-2.

Fig. 18c shows the resulting modified parabola at e_3 as generated by Mode 1 and by Mode 2. It may be seen that the two traces practically merge. They could be made indistinguishable from each other by making a slight change in one of the feedback resistors involved.

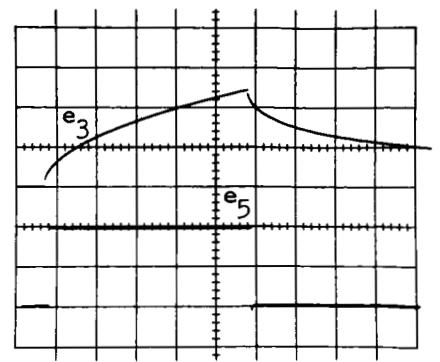
Fig. 18d shows e_3 before (upper trace) and after (lower trace) modification to simulate the temperature effects on the thin-film sensor. The lower trace in Fig. 18e illustrates the erroneous character of the heat flux calculated by an electrical analog (e_5) as the sensor experiences these high-temperature effects. The correct value of e_5 as would be calculated under ideal conditions is also shown for comparison.

Fig. 18f shows the final results after correcting the voltage e_3 . The traces shown are for the analog output voltage e_5 . The lower trace shows the result of compensation with the PSQ network. This is to be compared to the middle trace which is the heat flux for ideal conditions. It may be observed that the lower trace is at the correct level of 0.8 times the value of e_5 for the ideal case, the coefficient 0.8 being the low voltage attenuation K_c of the PSQ network. The slight curvature of the trace is the expected result of the approximations used in generating the modified parabola.

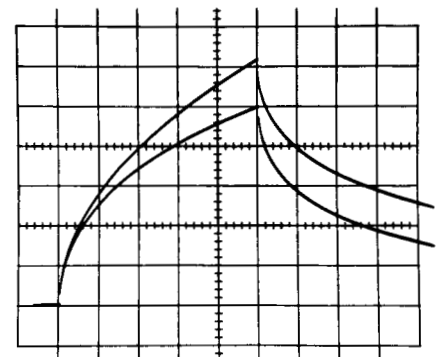
The upper trace of Fig. 18f shows the corresponding result for the varistor



(a)

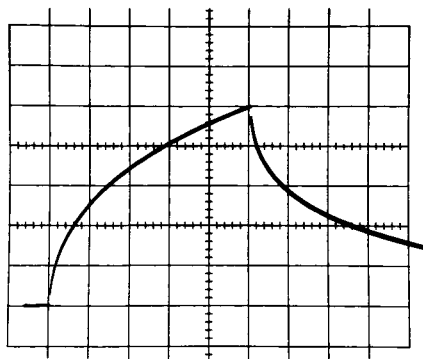


(b)

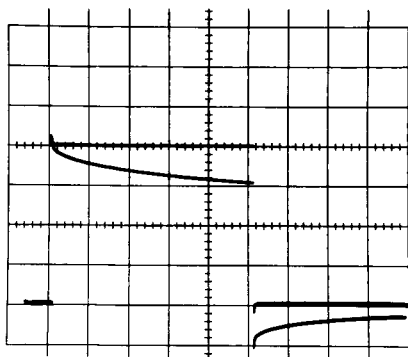


(d)

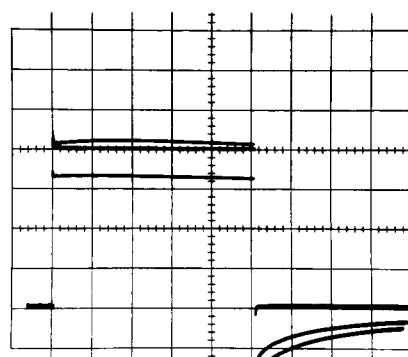
Figure 18. Experimental Results from Demonstrator Unit
Sweep Rate: 5 msec/cm



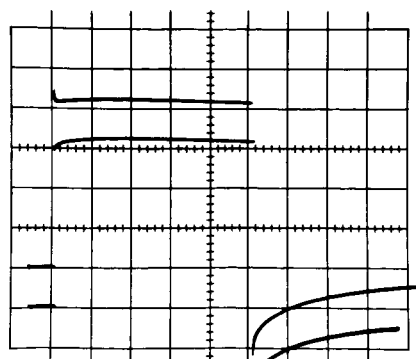
(c)



(e)



(f)



(g)

compensator. This trace is shown at twice the vertical scale sensitivity of the other two. Since $K_C = 0.516$ for the varistor network, the trace deflection should be $2 \times 0.516 = 1.03$ times that of the middle trace, the heat flux for ideal conditions. This also is seen to be closely realized. The varistor compensator produces a greater curvature in the trace for e_5 than the PSQ compensator. It simply does not perform the operation given in Eq. (20) as accurately as the PSQ compensator does.

The input impedance of the electrical analog unit changes over a wide range during a run. Initially, when the input signal is changing at an infinite rate, the impedance is a resistance of 20,000 ohms. This increases to more than a meg-ohm during the run. The effect of this variable loading on the varistor network is uncertain. Consequently, a high impedance follower, A-4, was included in the circuitry. The results of operation with and without A-4 are shown in Fig. 18g. The upper trace shows the results (voltage e_5) with varistor compensation and with A-4 coupled in, as was standard practice in using the varistor compensator. The lower trace shows the same thing with A-4 removed from the circuit and the output of the varistor network introduced directly into the analog network. It is evident that except at the earliest moments the loading effect is small.

SECTION FOUR
OPERATION IN CONJUNCTION WITH ANALOG UNIT

The operational use of a compensator unit requires it to be connected between the excitation network of the thin-film sensor and the electrical analog network. A scaling amplifier A is included ahead of the compensator, as shown in Fig. 19. This amplifier serves two purposes. First, it prevents the compensator from loading the sensor network and second, it provides a convenient means of adjustment to ensure that the compensator operates precisely at its design voltage. This latter requirement is ensured by setting the gain A, which is done by adjusting potentiometer R_2 . From Eq. (25) the required gain is found to be

$$A = K_N B \quad (35)$$

where $B = 1/30$ volt/ $^{\circ}\text{C}$ for the present designs.

Calibrations are normally made by chopping a dummy load resistor across a precision resistor to produce a specified value ΔR_g . For the particular scheme shown in Fig. 19 the calibrator box is connected in place of the gage when the phone jack is plugged in. The resistance increment is related to the indicated surface temperature rise that is to be simulated, by Eq. (14), where Φ applies to the particular gage used in the test.

The basis for generating the oscilloscope calibration trace in terms of heat flux is given by Eq. (13) of Ref. 13, which describes the transfer function of the electrical analog for a sinusoidally varying input, $T_s(t) = T_1 e^{j\omega t}$:

$$q(t) = \beta_o \sqrt{j\omega} T_s(t) \quad (36)$$

The phase angle is 45° , and the amplitude ratio is

$$\frac{q_1}{T_1} = \beta_o \sqrt{\omega} \quad (37)$$

where we have put $q_s = q_1 e^{j(\omega t + \phi)}$, thus defining q_1 . For a given value of β_o there is one particular frequency for which the amplitude ratio is unity. To illustrate, for the value $\beta_o = 0.074$ btu/ft²sec^{1/2}°F, the frequency in question is

$$f = \frac{1}{2\pi\beta_o^2} = \frac{1}{2\pi(0.074)^2} = 29.1 \text{ cps} \quad (38)$$

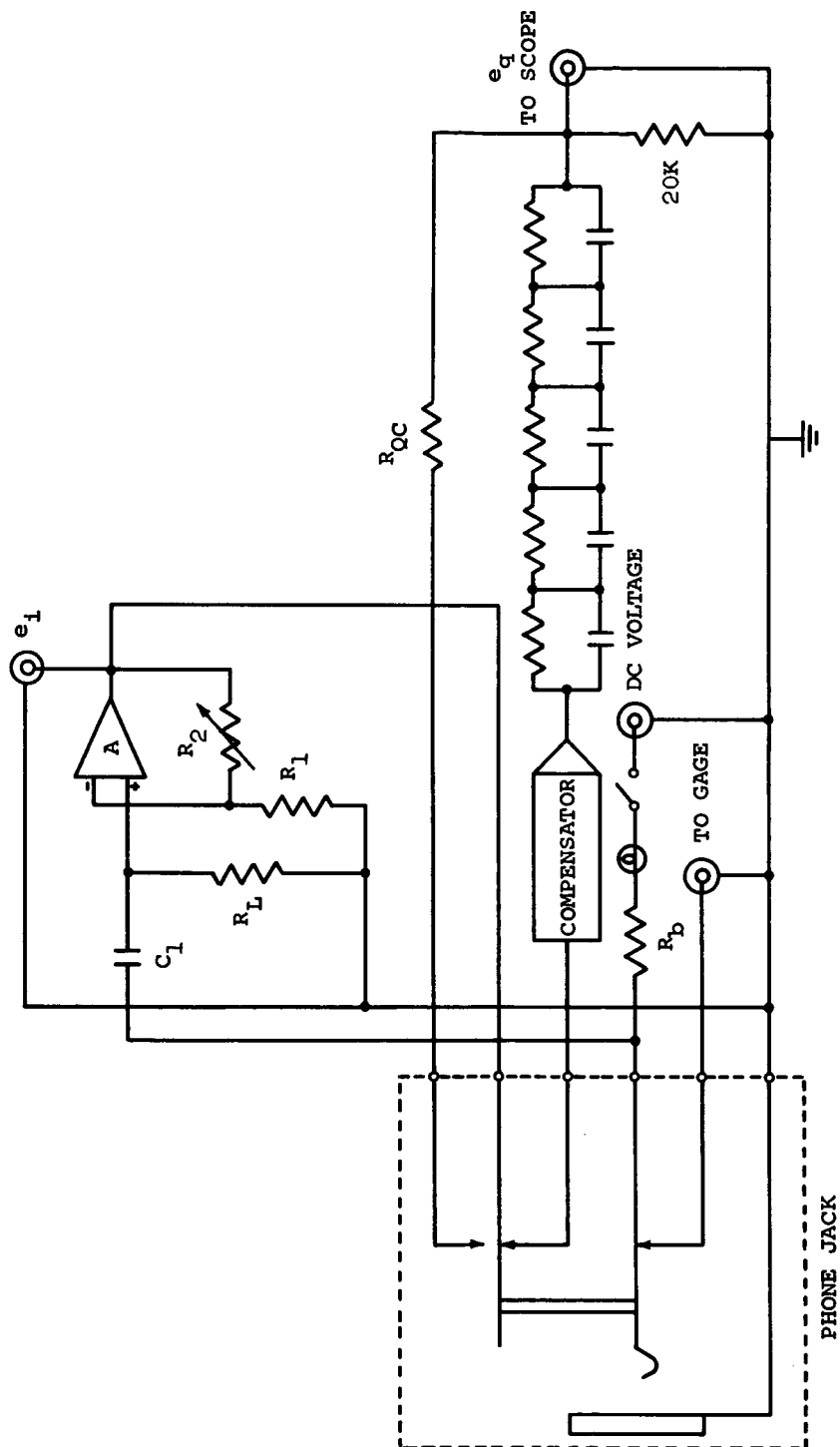


Figure 19. Schematic of Modified Analog Unit

This means in effect that a 29.1 cps calibration signal representing a 1°F temperature rise will also represent the calibration for one unit of heat flux, the units being $\text{btu/ft}^2\text{sec}$.

In practice, sinusoidal calibration signals are not used. Instead, the attenuation of the analog network at this reference frequency is duplicated by a voltage divider switched in for the purpose. Square-wave calibration signals may then be used. The voltage divider is set up to produce the same attenuation (phase lag is not a factor) as the analog network at the reference frequency. This amounts simply to switching in a fixed resistor R_{QC_0} in place of the five R-C sections of the analog. The required value of R_{QC_0} depends on the frequency scaling of the analog and on the value of the shunt resistor, normally 20,000 ohms. The attenuation factor is then

$$K_{QC_0} = \frac{20,000}{20,000 + R_{QC_0}} \quad (39)$$

Addition of the compensator unit into the operating network introduces an attenuation K_c . The calibration signal must therefore be attenuated by this same factor, i.e. $K_{QC} = K_c K_{QC_0}$. The required value for R_{QC} is then

$$R_{QC} = \frac{20,000 + R_{QC_0}}{K_c} - 20,000 \quad (40)$$

The system calibration is now carried out in the usual manner, but with the addition of the further step of setting the gain of the scaling amplifier, which must be reset any time a change, such as changing gages or altering the supply voltage level, is made within the sensor excitation network. The steps are:

- (i) Determine the value of ΔR_g to be simulated, from

$$\Delta R_g = \phi q_c \quad (41)$$

where q_c is the desired calibration trace deflection in heat transfer units. The value of the dummy load resistor required in the calibration circuit will then be determined.

- (ii) Adjust potentiometer R_2 of Fig. 19 so that the output of amplifier A is

$$e_i = B q_c \quad (42)$$

where it is to be remembered that numerical equivalence has been assigned between temperature and heat flux units.

(iii) Ascertain that R_{QC} correctly reflects the presence of the compensator unit through Eq. (40), where R_{QC_0} is the conventionally determined value of the resistance substituted for the analog network sections.

SECTION FIVE
CORRECTION OF UNCOMPENSATED HEAT FLUX MEASUREMENTS

5.1 General Solution

We assume now that heat flux measurements are made with a conventional analog unit, without compensation. The input to the analog unit is then the indicated temperature $T_i(t)$ and the output the uncorrected heat flux $q_u(t)$. Our objective here is to find a convenient means for obtaining the corrected heat flux $q_c(t)$ directly from $q_u(t)$.

The compensation derived earlier is carried out on $T_i(t)$, that is, the function $\theta_w^{(o)}(t)$, which when supplied to a linear analog will produce the corrected solution $q_c(t)$, is given by Eq. (17). We need, therefore, a convenient relationship between the analog input and output so that $T_i(t)$ can be found from $q_u(t)$, and then $\theta_w^{(o)}(t)$ calculated in order to find $q_c(t)$.

The analog network is designed to approximate the transfer function relating the surface temperature of a semi-infinite solid, initially at constant temperature, to the surface heat flux, assuming one-dimensional, linear heat conduction. The general analytic solution for this problem is given, for example, in Ref. 6; however, this is expressed in integral form and not particularly well suited to our present needs. Instead, we find that both the surface temperature and heat flux can be written as related power series in $t^{1/2}$; see p. 63 of Ref. 6. This is a particularly useful form for representing the analog input and output data since in many applications the heat flux is essentially a constant, with the surface temperature proportional to $t^{1/2}$. For the shock tube wall case, the heat flux is proportional to $t^{-1/2}$, corresponding to constant surface temperature increment.

If we express the indicated surface temperature as

$$T_i(t) = a_0 + a_1 t^{1/2} + a_2 t + \dots + a_n t^{1/2n} + \dots \quad (43)$$

where a_0, a_1, \dots are constant coefficients, then the uncorrected heat flux is of the form

$$\begin{aligned} \frac{2}{\beta_0 \sqrt{\pi}} q_u(t) &= \frac{2}{\pi} a_0 t^{-1/2} + a_1 + \frac{4}{\pi} a_2 t^{1/2} + \frac{3}{2} a_3 t + \dots \\ &+ \frac{2}{\sqrt{\pi}} \frac{\Gamma(\frac{1}{2}n + 1)}{\Gamma(\frac{1}{2}n + \frac{1}{2})} a_n t^{(\frac{1}{2}n - \frac{1}{2})} + \dots \end{aligned} \quad (44)$$

where $\Gamma(n)$ is the Gamma function. The relationship between coefficients holds

in general, of course, for any surface temperature and heat flux expressed in this fashion.

To find $\theta_w^{(o)}$ we substitute Eq. (43) into Eq. (17) to get

$$\begin{aligned}\theta_w^{(o)}(t) = & a_o(1 + \epsilon a_o) + a_1(1 + 2\epsilon a_o)t^{\frac{1}{2}} \\ & + [a_2 + \epsilon(a_1^2 + 2a_o a_2)]t \\ & + [a_3 + 2\epsilon(a_o a_3 + a_1 a_2)]t^{\frac{3}{2}} + \dots\end{aligned}\quad (45)$$

where we have taken $\epsilon \equiv \lambda/\mathcal{J}_1$. Using the relationship between coefficients in Eqs. (43) and (44), we have that

$$\begin{aligned}\frac{2}{\beta_o \sqrt{\pi}} q_c(t) = & \frac{2}{\pi} a_o(1 + \epsilon a_o)t^{-\frac{1}{2}} + a_1(1 + 2\epsilon a_o) \\ & + \frac{4}{\pi} [a_2 + \epsilon(a_1^2 + 2a_o a_2)]t^{\frac{1}{2}} \\ & + \frac{3}{2} [a_3 + 2\epsilon(a_o a_3 + a_1 a_2)]t + \dots\end{aligned}\quad (46)$$

Additional terms in these series can easily be worked out if needed. Subtracting Eq. (44) from Eq. (46), we obtain

$$\begin{aligned}\frac{2}{\beta_o \sqrt{\pi}} [q_c(t) - q_u(t)] = & \frac{2}{\pi} \epsilon a_o^2 t^{-\frac{1}{2}} + 2\epsilon a_o a_1 \\ & + \frac{4}{\pi} \epsilon(a_1^2 + 2a_o a_2)t^{\frac{1}{2}} \\ & + 3\epsilon(a_o a_3 + a_1 a_2)t + \dots\end{aligned}\quad (47)$$

The first step in correcting heat flux data is to fit the series of Eq. (44) to the uncorrected data in order to determine the coefficients a_o, a_1, \dots . This can probably be done adequately by starting with several terms from the series and fitting them to the data using a least-squares procedure. If the fit is not within experimental accuracy, more terms can be added. The corrected heat flux $q_c(t)$ can then be found by inserting the coefficient values directly into Eq. (46) or (47).

5.2 Correction Under Constant Heat Flux Conditions

If the type of heating is known, the above method can be extended to obtain

simpler and more easily used correction formulas. Therefore, we will restrict our attention now to the common condition where the heating q_c is constant.

From Eq. (46), the coefficients become: $a_0 = 0$, $a_1 = 2q_c/\beta_0\sqrt{\pi}$, $a_2 = -\epsilon a_1^2$, $a_3 = 2\epsilon^2 a_1^3$, Therefore, from Eq. (45) we obtain the familiar relation

$$\theta_w^{(0)} = a_1 t^{1/2} = \frac{2q_c}{\beta_0\sqrt{\pi}} t^{1/2} \quad (48)$$

See Eq. (8). Using these results in Eq. (44), we get a power series in $\epsilon\theta_w^{(0)}$ for the ratio q_u/q_c . It can be shown that this series converges for $\epsilon\theta_w^{(0)} < 1/4$, which essentially is the range of applicability of the present compensation method. By evaluating this series over the range of $\epsilon\theta_w^{(0)}$ and using Eq. (48) we can find the inverse ratio, q_c/q_u , as a function of the parameter $2\epsilon q_u t^{1/2}/\beta_0\sqrt{\pi}$. All quantities in this parameter are known from the record of the uncorrected data so that the corrected heat flux can then be found directly.

To carry all terms in this power series is not, however, to be fully consistent with our earlier derivation of the compensation equations, where, effectively, terms of order $[\epsilon\theta_w^{(0)}]^2$ and higher have been neglected. If we then truncate the series after only two terms, we find

$$\frac{q_u}{q_c} = 1 - \frac{4}{\pi} \epsilon \theta_w^{(0)} = 1 - \frac{4}{\pi} \epsilon \frac{2q_c t^{1/2}}{\beta_0\sqrt{\pi}} \quad (49)$$

a quadratic in q_c . Solving for q_c , expanding the square root term, and again neglecting terms which are essentially of order $[\epsilon\theta_w^{(0)}]^2$ and higher, we obtain the convenient correction formula:

$$\frac{q_c}{q_u} = 1 + \frac{8\epsilon}{\beta_0\pi^{3/2}} q_u t^{1/2} \quad (50)$$

The difference between this simplified form for q_c/q_u and that obtained by using the entire power series is less than 0.7% for values of $8\epsilon q_u t^{1/2}/\beta_0\pi^{3/2}$ up to 0.19.

Eq. (49) describes the manner in which the indicated heat flux will vary with time. Starting at the correct value, the signal will subsequently droop below it by an amount proportional to $t^{1/2}$.

The correction formula, Eq. (50), is shown plotted in Fig. 20. In this plot the value of ϵ employed is consistent with parametric values employed in

preceding sections of this report, namely, $\epsilon = 0.25/300^\circ\text{C} = 0.000833^\circ\text{C}^{-1} = 0.000463^\circ\text{F}^{-1}$. The value of β_0 that has been used is $\beta_0 = 0.074 \text{ btu/ft}^2\text{sec}^{1/2}\text{F}$. Eq. (50) and, therefore, Fig. 20 apply identically only to the case of constant applied heat flux. Related material presented in Fig. 8 of Ref. 4 suggests that the magnitude of the correction factor does not vary greatly for different analytic variations of heat flux. We deduce from this that Fig. 20 may be used even when the heat flux deviates from a constant value.

A different type of high-temperature effect in thin-film thermometry occurs if the sensor is pre-heated (or cooled) so as to reside initially at other than room temperature conditions. Then the correction called for is the value of β applicable to the initial temperature condition of the gage rather than the room temperature value. If an analog unit is employed, the frequency given by Eq. (38) will be modified, and the associated value of R_{QC_0} must be changed correspondingly, otherwise a correction factor must be applied to the oscilloscope calibration traces. A correction curve for β to serve these purposes is given in Fig. 4.

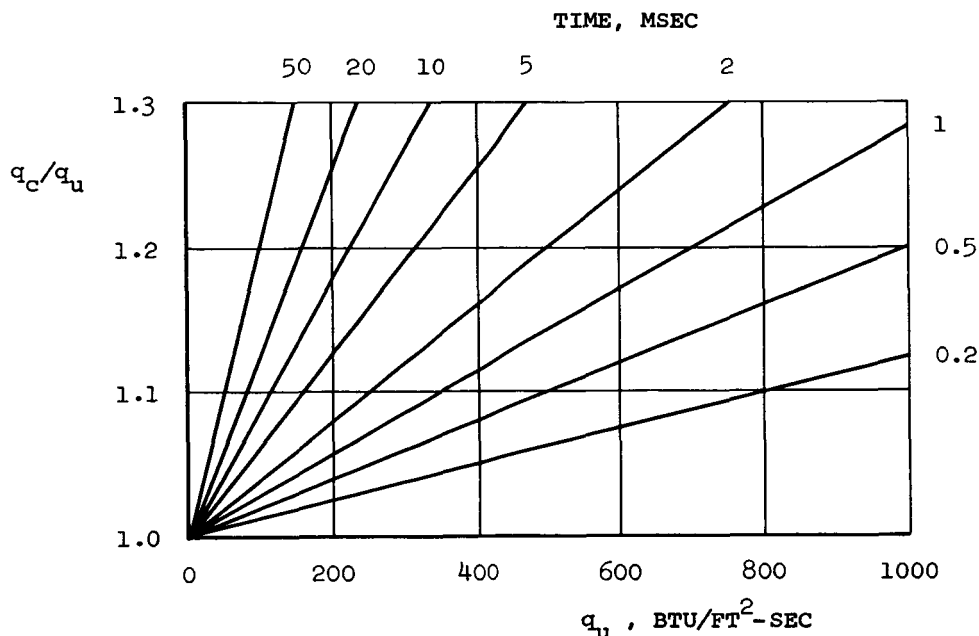


Figure 20

CONCLUSIONS AND RECOMMENDATIONS

A primary requirement of the present study was to determine the theoretical basis for making an on-line correction for temperature-dependent effects in thin-film thermometry. On the completion of this phase of the study it was concluded that it is possible to incorporate these effects in a single correction factor to be applied to the input voltage signal of an analog network. This correction factor covers the effects of temperature on: (i) thermal conductivity and thermal diffusivity of the substrate material, and (ii) thermal coefficient of resistivity of the thin-metallic-film resistance element. As opposed to results previously found, the correction for temperature effects on thermal diffusivity is not negligible.

Simple designs of compensating network are feasible. Experimental verification of this was shown in the course of the present investigation. A compensating network of the type developed here may be included in an operational unit without modifying normal practice except that one additional step is necessary in calibrating the system. The operation of the resulting network is not contingent on the applied heat flux conforming to a specific pattern.

A method is provided to correct raw heat transfer data for high temperature effects if the uncorrected heat flux history can be approximated by a power series in $t^{1/2}$. Explicit corrections are given in the case where the actual heat flux is reasonably constant.

Serious disagreement has been observed between one and another set of previously reported data regarding the effects of high temperature on the parameters of thin-film thermometry. The data furnished in the present report are of conventional origins and occupy the middle ground in comparison with the data given in Refs. 1-4. It is therefore recommended that the data provided herein be used for general application to platinum-on-Pyrex thin-film gages, at least until clarifying experiments have been conducted. Also, in the meantime, the widely accepted value of $0.074 \text{ btu/ft}^2\text{sec}^{1/2} \text{ }^\circ\text{F}$ for β should be retained.

A research program should be undertaken to resolve the discrepancies referred to in the previous paragraph and the experiments should be conducted so as to simulate closely the conditions of use of the gage. This means that the heat should be applied suddenly (say, by a strong electrical pulse). The program should be conceived to determine whether such factors as process, materials and source are significant and whether one of these is the cause of present disagreements. The valuable outcome of such research will be to upgrade the quality of heat transfer measurements especially under conditions of high heat flux.

REFERENCES

1. Somers, L. M., The Variation of $(k\rho c_p)^{1/2}$ with Temperature in "Pyrex", Cornell Aeronautical Laboratory, Inc., Report No. CAL-106, July 1961.
2. Bogdan, L., High Temperature, Thin-Film, Resistance Thermometers for Heat Transfer Measurement, Cornell Aeronautical Laboratory, Inc., Report No. HM-1510-Y-6, February 1963.
3. Hartunian, R. H., and Varwig, R. L., A Correction to Thin-Film Heat Transfer Measurements, Aerospace Corporation, Report No. TDR-594(1217-01)TN-2, May 1, 1961.
4. Walenta, Z. A., Analogue Networks for High Heat-Transfer Rate Measurements, University of Toronto, Institute for Aerospace Studies, UTIAS Technical Note No. 84, November 1964.
5. Reece, J. W., Temperature-Dependent Materials Properties in Thin-Film Thermometry and Theory for Their Compensation, Therm Advanced Research, Inc., TAR-RM 6501, October 1965.
6. Carslaw, H. S., and Jaeger, J. C., Conduction of Heat in Solids, Oxford University Press, 1959.
7. Schmitz, L. S., Nonlinear Analog Network to Convert Surface Temperature to Heat Flux, Cornell Aeronautical Laboratory, Inc., Report No. 130, June 1963.
8. Vidal, R. J., Model Instrumentation Techniques for Heat Transfer and Force Measurements in a Hypersonic Shock Tunnel, Cornell Aeronautical Laboratory, Inc., Report No. AD-917-A-1, February 1956.
9. Rose, P. H., and Stark, W. I., Stagnation Point Heat Transfer Measurements in Dissociated Air, Journal of the Aeronautical Sciences, Vol. 25, No. 2, February 1958.
10. Kingery, W. D., Heat Conductivity Processes in Glass, Journal of the American Ceramic Society, Vol. 44, No. 7, 302-304, July 1961.
11. Gardon, R., A Review of Radiant Heat Transfer in Glass, Journal of the American Ceramic Society, Vol. 44, No. 7, 305-312, July 1961.
12. Reece, J. W., A Correction Formula for Thin-Film Resistance Thermometers, Therm Advanced Research, Inc., TAR-TR 6406, October 1964.
13. Skinner, G. T., Analog Network to Convert Surface Temperature to Heat Flux, Cornell Aeronautical Laboratory, Inc., Report No. CAL-100, February 1960.
14. Kovach, L. D., and Comley, W., Nonlinear Transfer Functions with Thyrite, IRE Transactions on Electrical Computers, Vol. EC-7, No. 2, 91-97, June 1958.

APPENDIX A

VARIATION OF PROPERTIES OF THIN-FILM SENSOR MATERIALS WITH TEMPERATURE

A.1 General

The prevailing practice in the construction of thin-film resistance thermometers is to use #7740 Pyrex glass for the substrate material and a brush-applied solution of platinum for the resistance element. The solution commonly used is Hanovia #05-X Liquid Bright Platinum. When baked at a temperature of 1200°F-1250°F, the platinum is deposited and bonds to the glass substrate. Proper results require that certain standards of performance and technique be met in the fabrication process². Excellent adhesion of the platinum film to the pyrex base is then obtained, and the electrical properties of the gage are stable. As a result, generally excellent results have been obtained in use and have upheld the prevailing choice of materials.

A discussion of the pertinent physical properties was given in Ref. 5 , and the results are summarized in this section.

A.2 Physical Properties of #7740 Pyrex

The primary physical properties of Pyrex with which we are concerned are density, specific heat, and thermal conductivity, and particularly their variation with temperature.

(i) Density: $\rho = 2.23 \text{ gm/cm}^3$.

(ii) Specific Heat: The variation of the specific heat of Pyrex with temperature is shown in Fig. 1 . This curve differs little from that for fused silica, for which excellent agreement between experimental and theoretical values of specific heat has been shown. The small difference from the comparable data for fused silica is attributed to the small amounts of oxides added to make Pyrex. Consequently, we regard this plotted data as being reliable.

(iii) Thermal Conductivity: Reasoning along theoretical lines, Kingery¹⁰ has shown that the thermal conductivity of glass should be approximately proportional to its specific heat. We may take this as indicating that the thermal conductivity should increase with temperature as the specific heat does. This is also to say that the diffusivity should be relatively insensitive to temperature.

This expectation tends to be borne out by recent experimental data. The more recent data also show an improved consistency compared to past results. This evidently reflects improved experimental techniques designed to minimize the influence of radiation conductivity, an effect that has undoubtedly crept into and compromised the value of much data taken in the past¹¹.

The data given in Fig. 2 , repeated from Ref. 5 , are believed to be free of this effect and to be reliable to much the same degree as the corresponding specific heat data of Fig. 1 .

Radiation conductivity, that is, the volume phenomenon of progressive absorption and reradiation of heat, is not believed to play a significant role in thin-film thermometry. Therefore it is appropriate that this effect be excluded from the data to be used, as we presume to have done. A temperature limit of 600°K is implied in Fig. 2 . Above this the situation is obscured by the approaching tendency of radiation conductivity to dominate the experimental results.

(iv) Derived Properties: The preceding data enables the thermal diffusivity to be calculated from the definition $K = k/\rho c$. The results are given in Fig. 3 and show the expected mild dependence on temperature.

A parameter frequently encountered in thin-film thermometry is $\beta \equiv \sqrt{k\rho c} = k/\sqrt{K}$. For purposes of reference the variation of β with temperature for the present data is given in Fig. 4 . Various experimenters¹⁻⁴ have used an electrical pulsing technique to evaluate β for thin-film gages. Their overall results, although they bracket the curve given in Fig. 4 , differ among themselves quite widely. This is in fact a major reason why preference has been given here to data obtained by more conventional techniques. If there are other factors that need to be taken into account, it is proposed that this be investigated methodically in the future.

The room temperature value of β_0 commonly agreed on by Vidal⁸, Sommers¹, Bogdan² and Hartunian³ is $\beta_0 = 0.074 \text{ btu/ft}^2 \text{ sec}^{1/2} \text{ } ^\circ\text{F}$. The present data for Pyrex gives a value 7% lower than this, but the reasons for this disagreement are not known.

A.3 Properties of the Platinum Thin-Film Resistance Element

Resistance measurements to 1000°F were performed by Bogdan², who found that the resistance-temperature function of the platinum film, as deposited on Pyrex, is nonlinear. The resulting gage sensitivity dR/dT varies linearly with temperature as shown in Fig. 5 . The relation given by Bogdan as the best fit to his data is

$$\frac{(dR/dT)}{(dR/dT)_{70^\circ\text{F}}} = 1.018 - 2.59 \times 10^{-4} T(^{\circ}\text{F}) \quad (51)$$